



# U–Pb apatite geochronology shows multiple thermal overprints within the Neoproterozoic foreland basement of the Faroe–Shetland Terrane

R. A. Strachan<sup>1\*</sup>, C. L. Kirkland<sup>2</sup>, A. J. Finlay<sup>3</sup>, D. S. Wray<sup>4</sup>, J. H. Metcalfe<sup>1</sup>  
and R. E. Holdsworth<sup>5</sup>

<sup>1</sup> School of the Environment, Geography and Geosciences, University of Portsmouth, Portsmouth PO1 3QL, UK

<sup>2</sup> Timescales of Mineral Systems Group, School of Earth and Planetary Sciences, Curtin University, Perth, WA 6845, Australia

<sup>3</sup> Chemostrat Ltd, 1, Ravenscroft Court, Buttington Enterprise Park, Welshpool SY21 8SL, UK

<sup>4</sup> School of Science, Faculty of Engineering and Science, University of Greenwich, Chatham Maritime ME4 4TB, UK

<sup>5</sup> Department of Earth Sciences, University of Durham, Durham DH1 3LE, UK

RAS, 0000-0002-9568-0832

\*Correspondence: [rob.strachan@port.ac.uk](mailto:rob.strachan@port.ac.uk)

**Abstract:** The Neoproterozoic foreland basement of the Faroe–Shetland terrane (FST) displays abundant evidence for isotopic resetting of U–Pb systems in apatite between *c.* 1800 and 200 Ma, interpreted to result from episodic heating pulses associated with regional-scale tectonic events. Major apparent age peaks of *c.* 1800–1600 Ma broadly correspond to the timing of Nagssugtoqidian–Laxfordian orogenesis >225 km further south. These are thought to reflect widespread heating during late- to post-orogenic delamination that affected a wide area of the orogenic foreland and resulted in a low to middle greenschist-facies static overprint, affecting much of the FST basement. Late- to post-orogenic delamination might also account for major apparent age peaks at *c.* 1300–1100, 800 and 500–400 Ma, corresponding to, respectively, Grenvillian, Knoydartian and Caledonian orogenic events. However, east-dipping seismic reflectors in the basement west of Shetland may represent the northward extension of the Grenvillian Outer Hebrides Thrust (Zone) and/or Caledonian thrusts and so perturbation of isotherms during west-directed thrusting could therefore also account for these apparent age peaks. Minor apparent age peaks of *c.* 700, 600, 350 and 200 Ma are most easily interpreted as resulting from enhanced heat flux that accompanied periods of crustal extension prior to and following the Caledonian orogeny.

**Supplementary material:** Supplementary tables are available at <https://doi.org/10.6084/m9.figshare.c.7278061>

**Received** 10 January 2024; **revised** 20 May 2024; **accepted** 29 May 2024

The traditional division between an orogen and its foreland is largely structurally based and arises from the identification of a basal thrust separating the deformed and metamorphosed orogenic wedge from a largely undeformed and unmetamorphosed footwall. However, this distinction may not provide a complete picture of orogenic activity, as thermal effects can extend far into the foreland. Thrusting can drive hot fluids towards orogenic forelands, and this process may lead to fluid–rock interaction and the development of mineral deposits (e.g. Oliver 1986; Craw *et al.* 2002; Mark *et al.* 2007). Textural features in datable minerals indicative of alteration by fluids include evidence for dissolution and regrowth of apatite (Kirkland *et al.* 2018b), and metamict textures in zircon frequently accompany fluid alteration in those crystals (Larsen and Tullborg 1998; Morris *et al.* 2015). Thermal overprinting of foreland rocks may also result from burial beneath orogenic thrust wedges (Johnson *et al.* 1985; Thigpen *et al.* 2021; Skipton *et al.* 2022) or heating associated with late- to post-orogenic extension (Gillespie *et al.* 2022). A wide range of low- to medium-temperature isotopic techniques can be used to assess the degree to which foreland rocks have been thermally overprinted and also to constrain the timing of authigenesis.

In this case study, we examine the thermal evolution of an extensive tract of Neoproterozoic orthogneisses, the Faroe–Shetland terrane (FST) which underlies an offshore region in the North Atlantic (Fig. 1a). The FST is part of the foreland to both the Paleoproterozoic Nagssugtoqidian orogen to the south, which includes the Lewisian Complex of NW Scotland (Kolb 2014; Holdsworth *et al.* 2019; Kinny *et al.* 2019), and the Ordovician–

Silurian Caledonian orogen to the east of the Moine Thrust Zone (Chew and Strachan 2014). Published petrological and isotopic data from the FST have largely been obtained by analysis of borehole samples. U–Pb zircon dating has established the ages of its orthogneissic protoliths, but little is known about the subsequent thermal history. The U–Pb system in apatite has a closure temperature of around 375–550°C (Chew and Spikings 2015) meaning that it is ideal for investigating the medium-temperature evolution of metamorphic basement rocks. We summarize published and new petrological data and report new U–Pb apatite analyses from 11 samples, all of which have yielded U–Pb zircon ages (Finlay *et al.* 2023). Ten of these samples were taken from the FST basement and one from a Caledonian intrusion located east of what is interpreted as the northern continuation of the Moine Thrust (Fig. 1a). These new U–Pb apatite ages correspond closely to the timing of tectonothermal events within the orogenic hinterlands to the south and east. This prompts discussion of the possible mechanisms by which this and other foreland basement terranes might be thermally overprinted.

## Regional setting

Archean basement is extensively exposed in NW mainland Scotland and the Outer Hebrides and underlies a large offshore tract north of mainland Scotland and west of Shetland (Figs 1a and 2; Park 2005; Richie *et al.* 2011). This crust represents a fragment of Laurentia that was juxtaposed with Baltica and Avalonia during the Early Paleozoic Caledonian orogeny, and then separated from North

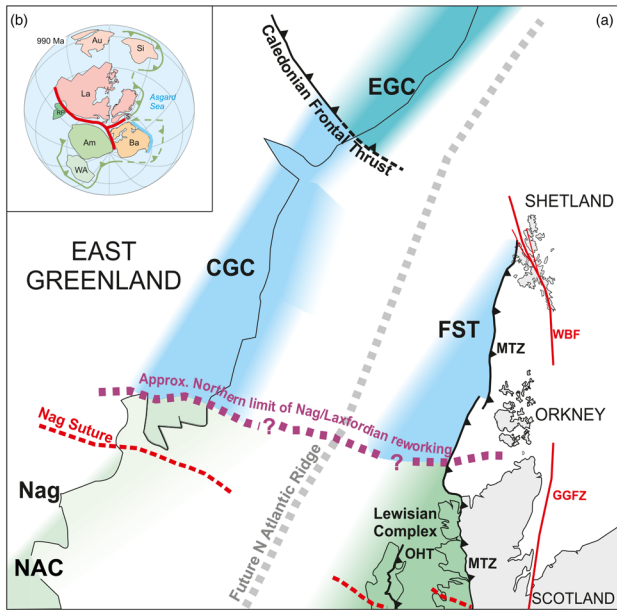


**Fig. 1.** (a) Simplified map showing the major age provinces within the northern British Isles and SE Greenland in a pre-Mesozoic drift configuration. FST, Faroe-Shetland terrane; OHT, Outer Hebrides Thrust; MTZ, Moine Thrust Zone; GGFZ, Great Glen Fault Zone; WBF, Walls Boundary Fault; Nag, Nagssugtoqidian orogen; CGC, Central Greenland (Rae) Craton; NAC, North Atlantic Craton; EGC, East Greenland Caledonides. (b) Palaeogeographical reconstruction for c. 990 Ma. Red line shows the extent of the collisional Grenvillian-Sveconorwegian orogen and its northern arm between Laurentia and Baltica; green lines with triangles show peri-Rodinian subduction zones; blue line indicates a passive margin adjacent to (present-day) northern Baltica. Au, Australia; Si, Siberia; La, Laurentia; S, Scotland (including Shetland); Ba, Baltica; RP, Rio Plata craton; Am, Amazonia; WA, West African craton. Sources: (a) modified from Holdsworth *et al.* (2019); (b) modified from Cawood *et al.* (2016).

America and Greenland during the late Mesozoic to Cenozoic opening of the North Atlantic Ocean. It forms the 'Hebridean foreland' to the Caledonian orogen, which is limited to the west by the east-dipping Moine Thrust (Figs 1a and 2).

The Archean basement west of the Moine Thrust comprises two main provinces. The first is the Lewisian Gneiss Complex of NW mainland Scotland and the Outer Hebrides, also commonly referred to as the 'Hebridean terrane'. This is dominated by tonalite-trondhjemite-granodiorite (TTG) orthogneisses, which have yielded evidence for crustal accretion at c. 3.1–2.7 Ga and subsequent granulite-facies metamorphism at 2.7 Ga (e.g. Whitehouse 1989; Kinny and Friend 1997; Whitehouse *et al.* 1997; Love *et al.* 2004; Kinny *et al.* 2005; Kelly *et al.* 2008; Wheeler *et al.* 2010; Whitehouse and Kemp 2010; Crowley *et al.* 2015). These were later subject to further high-grade metamorphism at 2.5 Ga, dyke intrusion at 2.4 Ga and variably intense Paleoproterozoic (Laxfordian) ductile reworking at 1.8–1.65 Ga (e.g. Whitehouse 1993; Corfu *et al.* 1994; Friend and Kinny 2001; Whitehouse and Bridgewater 2001; Mason 2012, 2016; Goodenough *et al.* 2013; Davies and Heaman 2014). Further north, the second basement province is represented by the mainly offshore FST, which is largely understood from the study of borehole samples (Chambers *et al.* 2005; Holdsworth *et al.* 2019), although a small area is exposed in NW Shetland (Kinny *et al.* 2019) (Figs 1a and 2). The FST basement is lithologically similar to the Lewisian Gneiss Complex, and U–Pb zircon dating has yielded comparable orthogneiss protolith ages of c. 2.8–2.7 Ga (Fig. 2; Supplementary Table S1; Chambers *et al.* 2005; Richie *et al.* 2011; Holdsworth *et al.* 2019; Finlay *et al.* 2023). Field evidence from Shetland suggests that emplacement overlapped deformation and high-grade metamorphism (Kinny *et al.* 2019), and hence gneissification within the FST probably also occurred during the Neoproterozoic. However, the two provinces differ in one important respect: U–Pb zircon analyses within the FST show no evidence of

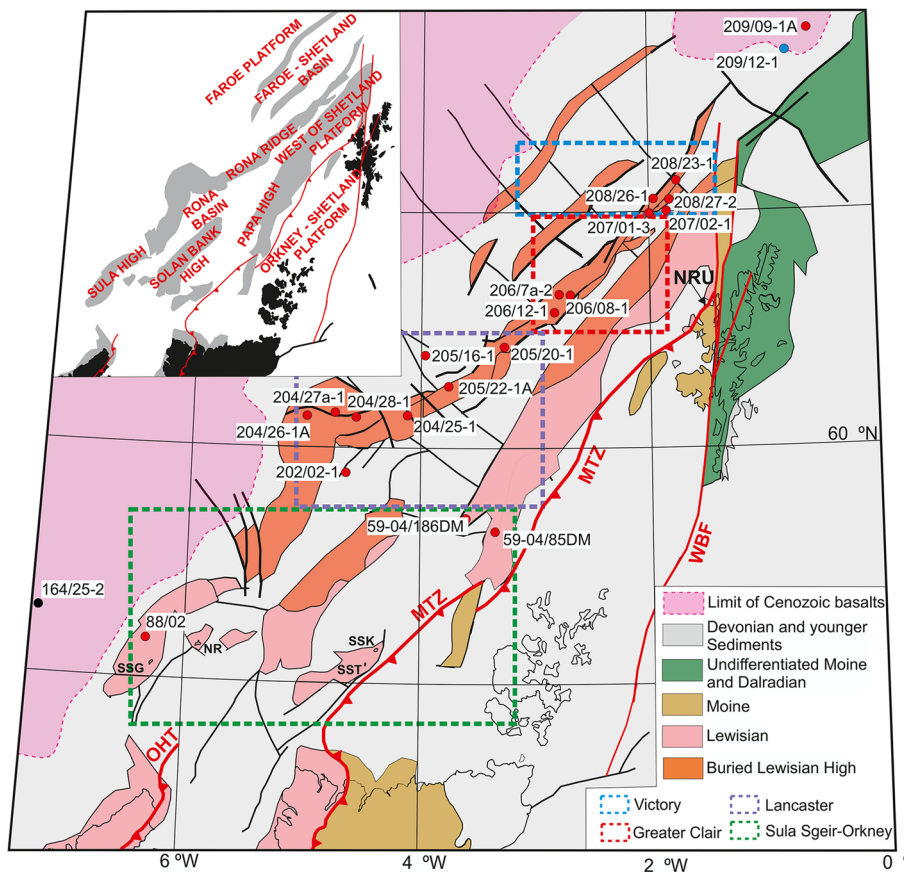


**Fig. 2.** Map showing basement distribution at seabed, structural elements (grey lines) and locations of wells referred to in the text and Supplementary material Table S1. The colours of the wells indicate the age of the basement penetrated: red dots, Archean; black dot (164/25-2), Late Mesoproterozoic; blue dot (209/12-1), Silurian (granite) (sources are listed in Supplementary material Table S1). Dashed boxes show locations of oilfields. OHT, Outer Hebrides Thrust; MTZ, Moine Thrust Zone; WBF, Walls Boundary Fault; NRU, North Roe-Uyea area, Shetland; SSK, Sule Skerry; SST, Sule Stack; NR, North Rona; SSG, Sula Sgeir. Source: modified from Holdsworth *et al.* (2019).

the high-grade Paleoproterozoic reworking that characterizes large parts of the Lewisian Gneiss Complex or indeed any younger high-temperature thermal overprint.

Prior to the opening of the North Atlantic Ocean, the Lewisian Gneiss Complex and the FST were contiguous with the basement terranes of SE and East Greenland (Fig. 1a). Collision of the upper plate North Atlantic Craton and the lower plate Central Greenland Craton formed the Nagssugtoqidian orogenic belt during the Paleoproterozoic (Fig. 1a; Kolb 2014). The Lewisian Gneiss Complex has been correlated with the Nagssugtoqidian belt and the FST with the Central Greenland (Rae) craton (Fig. 1a; Kalsbeek *et al.* 1993; Friend and Kinny 2001; Park 2005, 2022; Richie *et al.* 2011; Holdsworth *et al.* 2019; Kinny *et al.* 2019). A northern ‘front’ of Nagssugtoqidian reworking is thought to be located between northern mainland Scotland and Orkney, separating the two basement provinces (Fig. 1a). By analogy with the northern margin of the Nagssugtoqidian belt in SE Greenland, this front probably dips moderately southwards. The FST thus represents part of the foreland to the Nagssugtoqidian orogen, which formed during the assembly of the Columbia (or Nuna) supercontinent (e.g. Rogers and Santosh 2002; Evans and Mitchell 2011).

After partial break-up of Columbia and the rifting of Laurentia and Baltica post *c.* 1265 Ma, renewed convergence of these two cratons and Amazonia resulted in the Grenvillian–Sveconorwegian orogeny (1.2–1.0 Ga), a culminating event in the formation of the Rodinia supercontinent (Fig. 1b; Li *et al.* 2008). In northern Scotland, the Outer Hebrides Thrust was initiated (Imber *et al.* 2002; Metcalfe *et al.* 2024) and Neoproterozoic–Mesoproterozoic basement inliers within the Caledonides were reworked at high metamorphic grades (Sanders *et al.* 1984; Walker *et al.* 2016, 2021; Strachan *et al.* 2020b; Bird *et al.* 2023). The younger Tonian sedimentary sequences within the Caledonides of northern Scotland (traditionally referred to as ‘Moine’ (Fig. 2); but now subdivided into Wester Ross and Loch Ness supergroups; Krabbendam *et al.* 2021) contain evidence of Renlandian (*c.* 950–930 Ma) and Knoydartian (840–725 Ma) orogenesis (Rogers *et al.* 1998; Vance *et al.* 1998; Cutts *et al.* 2009, 2010; Cawood *et al.* 2015; Bird *et al.* 2018; Walker *et al.* 2021; Strachan *et al.* 2024), attributed to the development of the accretionary Valhalla orogen along the east Laurentian margin (Cawood *et al.* 2010). This was followed by a second supercontinent cycle. Following the Cryogenian–Ediacaran break-up of Rodinia and formation of the Iapetus Ocean, renewed continental convergence resulted in the Caledonian orogeny (*c.* 480–420 Ma; Pickering *et al.* 1988; Soper *et al.* 1992; Dewey and Strachan 2003). The Tonian metasedimentary successions and underlying Archean–Mesoproterozoic basement in northern Scotland were subject to amphibolite-facies metamorphism and thrust westwards at least 100 km onto the composite foreland formed by the Lewisian Gneiss Complex and the FST (Law *et al.* 2024 and references therein).

## Lithologies and petrology

The FST basement has mainly been sampled in British Geological Survey boreholes and seabed cores and commercial exploration wells located on two NE–SW-trending basement ridges, the Rona Ridge and the Solan Bank High. This basement is buried beneath mainly Mesozoic and younger sedimentary rocks and lies on the SE margin of the Faroe–Shetland basin (Fig. 2). The basement rocks are dominated by granodioritic to granitic orthogneisses with subordinate foliated granitoids and dioritic to mafic orthogneisses and amphibolites, as described in detail by Chambers *et al.* (2005), Richie *et al.* (2011) and Holdsworth *et al.* (2019, 2020). Orthogneisses in the NE of the Rona Ridge tend to be dominated by granitic and leucogranitic lithologies with minor granodiorite, whereas those in the SW are mainly granodioritic tonalitic and

dioritic with only minor granitic components (Finlay *et al.* 2023). The different orthogneiss types are typically interlayered on the decimetre to metre scale, and dioritic variants sometimes occur as enclaves. The small area of basement exposed onshore in NW Shetland is dominated by granitic gneiss with subordinate metagabbro intrusions (Kinny *et al.* 2019).

The following summary of the thin-section characteristics of the orthogneisses is derived largely from Holdsworth *et al.* (2019, 2020), based on samples obtained from the Clair (e.g. well 206/7a-2) and Lancaster (wells 205/21a-4Z, 205/21a-7 and 205/21-1A) fields (Fig. 2) but that are broadly representative of the wider FST. The gneisses are typically medium to coarse grained and weakly foliated to massive. Textural and mineralogical evidence for upper amphibolite- to granulite-facies regional metamorphism is indicated by (1) rare examples of charnockitic two-pyroxene metamorphic assemblages (as seen in 205/21a-7, for example; see fig. 5b of Holdsworth *et al.* 2020), (2) the ubiquitous preservation of tapered twinning in plagioclase and seriate–interlobate to amoeboid textures for plagioclase–quartz grain boundaries and (3) sector and fir-tree zoning textures within zircon grains (Chambers *et al.* 2005). Moderate- to low-intensity high-temperature deformation is also implied by development of marginal myrmekites and perthitic texture (Holdsworth *et al.* 2019). Textural and mineralogical evidence for a low-temperature, greenschist-facies overprint includes (1) weak development of subgrain rotation recrystallization textures, and deformation lamellae and undulose extinction in quartz, (2) alteration of calcic plagioclase to more albitic compositions together with replacement by sericite, epidote and clinozoisite and (3) variable pseudomorphing of pyroxene by aggregates of chlorite ± green biotite ± colourless amphibole ± talc ± epidote ± equigranular quartz ± carbonate, titanite and ore. In summary, the metamorphic history of the orthogneisses thus appears relatively simple, involving one phase of prograde upper amphibolite- to granulite-facies regional metamorphism that was followed by low-temperature greenschist-facies retrogression. The gneisses are also cut locally by late fine to ultrafine epidote–quartz veins, millimetre to centimetre thick phyllonites, and fault-related cataclasite and altered brown–green pseudotachylyte (e.g. see fig. 5e–g of Holdsworth *et al.* 2020).

## Previous geochronological and isotopic studies

U–Pb zircon data have been published from 30 samples of the offshore basement of the FST (Supplementary material Table S1; Fig. 2). The ages obtained mostly fall between *c.* 2.7 and 2.8 Ga, with only four yielding older ages of between *c.* 2.8 and 2.85 Ga (Chambers *et al.* 2005; Richie *et al.* 2011; Chemostrat 2014; Holdsworth *et al.* 2019; Finlay *et al.* 2023). Twenty-three of the analyses show some evidence of discordance, typically trending down towards Mesozoic lower intercept ages, which probably reflect lead loss during Phanerozoic basin development. A few define Neoproterozoic lower intercepts, but these have very large uncertainty. Cathodoluminescence imaging shows mainly primary magmatic zircon textures in grains that vary from equant to elongate prismatic with variably developed oscillatory igneous zonation patterns (e.g. Chambers *et al.* 2005, fig. 4.9; Holdsworth *et al.* 2019, fig. 7). Some grains have bright oscillatory zoned rims that are variously interpreted as either igneous in origin, probably produced by resorption in the melt, or the result of new growth during metamorphism. There is no petrographic evidence for widespread fluid activity; one sample containing common metamict grains yields a Neoproterozoic upper intercept age. Zircon Hf isotopes indicate that the orthogneisses formed from the recycling of Paleoproterozoic and Mesoarchean crust (Holdsworth *et al.* 2019). U–Pb zircon ages have been published from a further three samples that were obtained east of the probable northern continuation of the Moine Thrust

(Fig. 2): one from Neoproterozoic basement and two from Ordovician–Silurian granitoids (Supplementary material Table S1; Chambers *et al.* 2005; Chemostrat 2014; Finlay *et al.* 2023).

### Sample locations and descriptions

The samples analysed for the current study were all obtained from exploration wells and are described from SW to NE in a transect towards and across the Moine Thrust (Fig. 2). As detailed below, all samples yielded U–Pb zircon (LA-ICP-MS) ages (Finlay *et al.* 2023; Supplementary material Table S1).

#### 205/16-1

Two samples were taken from exploration well 205/16-1 (Fig. 2) at depths of 4275.3 and 4300–4314 m. The former is a medium-grained tonalitic gneiss (U–Pb zircon age  $2783 \pm 6$  Ma), comprising plagioclase, quartz, K-feldspar, clinopyroxene and biotite with accessory

sulfide, zircon and apatite. Secondary chlorite appears to pseudo-morph pyroxene, and fluorite occurs sporadically. Quartz–feldspar boundaries are strongly cusped–lobate (Fig. 3a). Quartz shows interlobate to amoeboid sub-grain boundaries, indicative of high-temperature (500–700°C) recrystallization via grain boundary migration (GBM) (Stipp *et al.* 2002; Passchier and Trouw 2005). Patchy undulose extinction and minor deformation lamellae also occur. Feldspar displays occasional bent twinning and a perthitic texture. The latter sample (U–Pb zircon age  $2742 \pm 6$  Ma) is a granodioritic gneiss although no thin section was available as the sample consisted entirely of cuttings that were amalgamated for U–Pb analysis. X-ray diffraction (XRD) analysis indicated that the sample comprises mainly plagioclase, quartz and K-feldspar (Finlay *et al.* 2023).

#### 206/7a-2

Two samples were taken from exploration well 206/7a-2 (Fig. 2) at depths of 2147.93 and 2598 m. The former is a coarse-grained

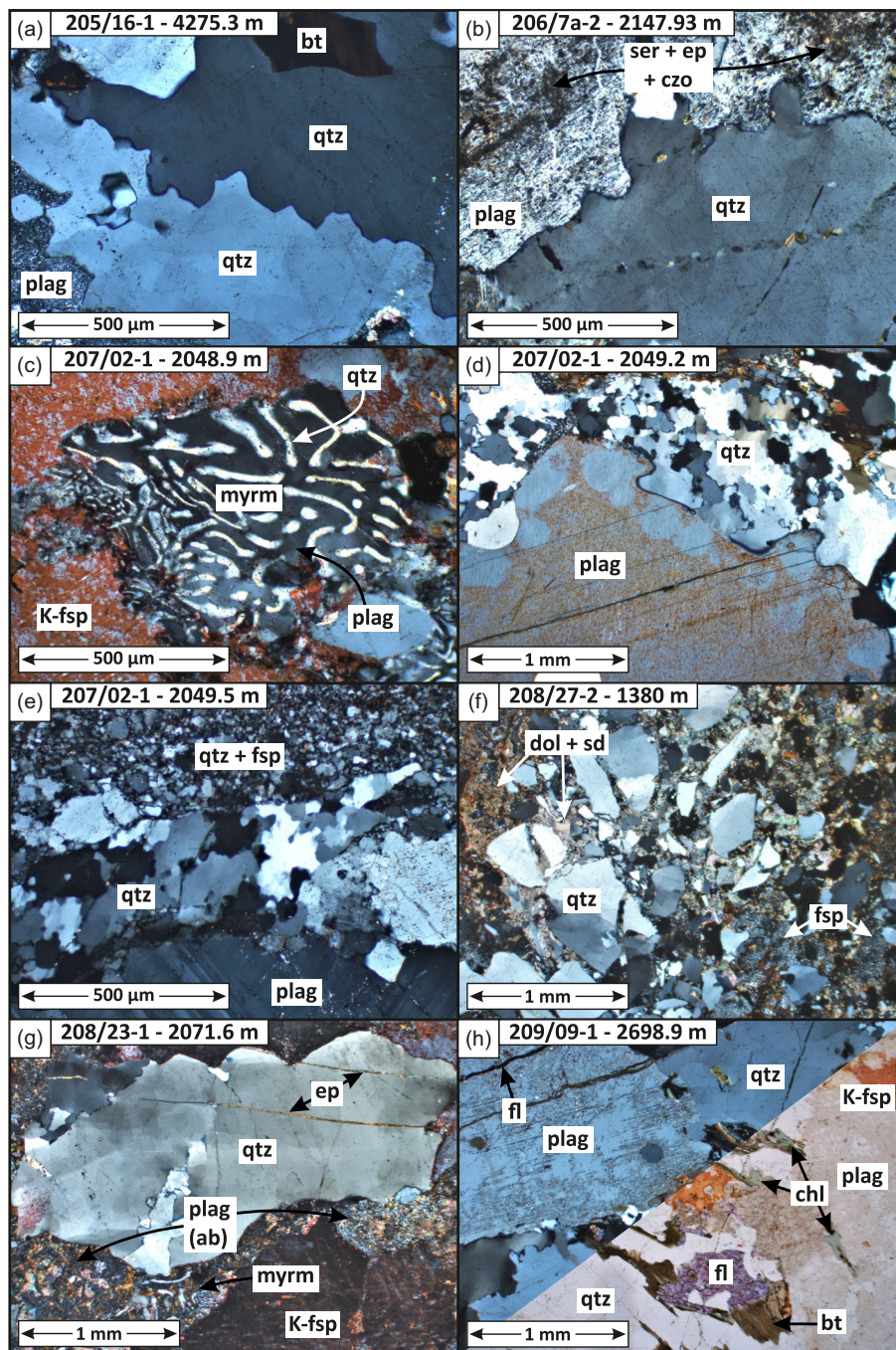


**Fig. 3.** Thin-section photomicrographs showing the textures exhibited from samples collected within each well. (a) Medium-grained tonalitic gneiss (205/16-1, 4275.3 m) in cross-polarized light (XPL) displaying a strongly cusped–lobate quartz–plagioclase grain boundary. Quartz shows interlobate to amoeboid sub-grain boundaries. (b) Coarse-grained tonalitic gneiss (206/7a-2, 2147.93 m) in XPL displaying a strongly cusped–lobate quartz–plagioclase grain boundary. Plagioclase is partially altered to ultrafine-grained sericite, epidote and clinozoisite. (c) Granitic gneiss (207/02-1, 2048.9 m) in plane-polarized light (PPL) displaying myrmekite developed along the grain boundary of K-feldspar. (d) Granitic gneiss (207/02-1, 2049.2 m) in XPL displaying a strongly cusped–lobate quartz–plagioclase grain boundary. Interlobate to amoeboid quartz indicates grain boundary migration recrystallization. (e) Granitic gneiss (207/02-1, 2049.5 m) in XPL. Bottom: relatively undeformed plagioclase; middle: interlobate to amoeboid quartz; top: ultrafine-grained quartz and feldspar recrystallized during medium-temperature (350–400°C) metamorphism. (f) Brecciated granitoid (208/27-2, 1380 m) in XPL displaying angular quartz and feldspar clasts among fine-grained precipitated dolomite and siderite. (g) Coarse-grained granitic gneiss (208/23-1, 2071.6 m) in XPL displaying subtle ‘chessboard’ extinction and sub-grain development in quartz, perthitic and myrmekitic K-feldspar and albitized plagioclase. Epidote veins can be seen to cross-cut the central quartz grain. (h) Granite (209/09-1, 2698.9 m) in XPL and PPL displaying partially sericitized plagioclase and interlobate quartz. Biotite alteration to chlorite and fluorite and fluorite veining is shown. ab, albite; bt, biotite; chl, chlorite; czo, clinozoisite; dol, dolomite; ep, epidote; fl, fluorite; fsp, feldspar; K-fsp, K-feldspar; myrm, myrmekite; plag, plagioclase; qtz, quartz; sd, siderite; ser, sericite.

tonalitic gneiss (U–Pb zircon age  $2851 \pm 18$  Ma), comprising plagioclase, quartz and pyroxene with accessory ore, apatite and zircon. The latter is a coarse- to very coarse-grained syenitic to granitic gneiss (U–Pb zircon age  $2726 \pm 8$  Ma) comprising K-feldspar, quartz, plagioclase, epidote and biotite with accessory apatite, ore and zircon. In both samples, quartz–feldspar boundaries are strongly cusped–lobate (Fig. 3b) and occasionally separated by marginal myrmekite within the latter sample. Quartz is characterized by GBM microstructures including amoeboid sub-grain boundaries and/or patchy or ‘chessboard’ extinction, both of which develop during very high-temperature ( $>700^\circ\text{C}$ ) metamorphism (Stipp *et al.* 2002; Passchier and Trouw 2005). K-feldspar commonly exhibits a perthitic texture and plagioclase is extensively altered to ultrafine grains of sericite, epidote and clinzoisite. Clots of chlorite and epidote may be a secondary replacement of biotite.

### 207/01-3

One sample was taken from exploration well 207/01-3 (Fig. 2) at a depth of 1423.4–1434.4 m. The sample is a granodioritic gneiss (U–Pb zircon age  $2734 \pm 16$  Ma), although no thin section was available as the sample consisted entirely of cuttings that were amalgamated for U–Pb analysis. XRD analysis indicated that the sample comprises mainly plagioclase, quartz and K-feldspar (Finlay *et al.* 2023).

### 207/02-1

Three samples were taken from exploration well 207/02-1 (Fig. 2), spaced  $<1$  m apart at depths of 2048.9, 2049.2 and 2049.5 m. The samples are all granitic gneisses and they yielded near identical U–Pb zircon ages of, respectively,  $2732 \pm 4$ ,  $2735 \pm 5$  and  $2735 \pm 4$  Ma (Finlay *et al.* 2023). They are therefore presumed to be the same meta-igneous body. It mainly comprises variable proportions of quartz, plagioclase and K-feldspar with accessory ore, apatite and zircon. K-feldspar has developed a perthitic texture internally and marginal myrmekite along grain rims (Fig. 3c) whereas plagioclase often displays bent twinning. Quartz shows extensive amoeboid sub-grain development and/or ‘chessboard’ extinction and forms strongly cusped–lobate grain boundaries with feldspar (Fig. 3d). All are classic GBM microstructures, which develop from very high-temperature ( $>700^\circ\text{C}$ ) metamorphism (Stipp *et al.* 2002; Passchier and Trouw 2005). Clots of biotite, chlorite, fluorite, epidote and ore appear to form pseudomorphs of an older mineral phase, most probably amphibole or pyroxene. In all three samples, narrow zones of fine-grained, recrystallized quartz and albite wrap quartz and feldspar porphyroclasts and are interpreted as the result of localized, medium-temperature ( $>350$ – $400^\circ\text{C}$ ) deformation that overprints a high-grade metamorphic assemblage (Fig. 3e).

### 208/27-2

One sample was taken from exploration well 208/27-2 (Fig. 2) at a depth of 1380 m. The sample is a brecciated granitoid (U–Pb zircon age  $2742 \pm 8$  Ma), comprising quartz, K-feldspar and plagioclase with accessory ore, apatite and zircon (Fig. 3f). Quartz occurs as angular clasts of variable grain size and often displays undulose extinction and/or amoeboid sub-grain boundaries (Stipp *et al.* 2002; Passchier and Trouw 2005). Plagioclase has been extensively sericitized and K-feldspar retains a perthitic texture. There is evidence for preservation of cusped–lobate quartz–feldspar grain boundaries pre-brecciation. Dolomite and siderite have been precipitated between the clasts and in fractures.

### 208/23-1

One sample was taken from exploration well 208/23-1 (Fig. 2) at a depth of 2071.6 m. The sample is a coarse-grained granitic gneiss

(U–Pb zircon age  $2782 \pm 6$  Ma), comprising quartz, K-feldspar and plagioclase with accessory ore, apatite and zircon. Quartz–feldspar boundaries are often highly cusped–lobate. Quartz displays patchy or ‘chessboard’ extinction (Fig. 3g) and amoeboid sub-grain boundaries, both classic GBM microstructures (Stipp *et al.* 2002; Passchier and Trouw 2005). K-feldspar exhibits a perthitic texture internally whereas plagioclase appears to have been completely albited and later replaced by precipitated fluorite and/or dolomite. Epidote veinlets cross-cut all mineral phases. These observations indicate that the early high-temperature gneissosity was overprinted by low-temperature ( $100$ – $150^\circ\text{C}$ ) metasomatism.

### 209/09-1A

One sample was taken from exploration well 209/09-1 (Fig. 2) at a depth of 2698.9 m. The sample is granitic in composition (U–Pb zircon age  $463 \pm 6$  Ma), comprising a coarse-grained recrystallized assemblage of quartz, plagioclase, biotite and K-feldspar with accessory ore, apatite and zircon (Fig. 3h). In thin section the sample appears largely equigranular but a gneissic compositional banding is evident in hand specimen. Quartz–feldspar grain boundaries are slightly cusped–lobate. Quartz shows undulose extinction and minor interlobate sub-grain boundaries. Plagioclase has been partially sericitized and may show minor bent twinning. Secondary fluorite, chlorite and epidote partially replace biotite and produce thin ( $<0.5$  mm), often discontinuous, veins that cross-cut all mineral phases.

In all the above samples, apatite is a ubiquitous accessory mineral that generally occurs as euhedral or prismatic, euhedral to anhedral homogeneous crystals up to  $500 \mu\text{m}$  in diameter with no evidence in petrographic thin sections or backscatter images of secondary recrystallization (Fig. 4). Apatite crystals are mainly enclosed within the primary minerals. These grain shapes and textural characteristics are consistent with a primary magmatic origin for the apatite.

## U–Pb analytical methods

Samples containing apatite grains were mounted in 25 mm resin pucks and polished to remove the surface of the grains. Grain identification was performed using SEM-ED-XRF wide-area mapping of the pucks. Isotopic analysis was undertaken at the University of Greenwich using a Thermo Scientific ICAP Q quadrupole ICP-MS instrument coupled to an ESI NWR 213 laser ablation system. Isotopic calibration was established and maintained via standard–sample bracketing throughout the measurement process using the McClure Mountain and Madagascar apatite standards (Chew and Donelick 2012; Thomson *et al.* 2012). A  $40 \mu\text{m}$  laser spot size was used with a 20 s blank measurement and a 40 s ablation of each grain. The laser had a nominal energy of  $4 \text{ J cm}^{-2}$  and a 10 Hz repetition rate, and the helium flow through the sample cell was  $600 \text{ ml min}^{-1}$ . The following isotopes were measured (dwell times per sweep):  $^{202}\text{Hg}$  (0.1 s),  $^{204}\text{Pb}$  (0.15 s),  $^{206}\text{Pb}$  (0.1 s),  $^{207}\text{Pb}$  (0.1 s),  $^{208}\text{Pb}$  (0.01 s),  $^{232}\text{Th}$  (0.01 s) and  $^{238}\text{U}$  (0.01 s). Raw data from the instrument were then processed using Iolite v4, using an in-house data reduction scheme that functions in a similar way to the VizualAge UcomPbine data reduction scheme (Chew *et al.* 2014).

## Calculation approach

Apatite U–Pb analyses typically define common–radiogenic mixing arrays in Tera and Wasserburg inverse concordia space (Tera and Wasserburg 1972) where the lower intercept may have age significance and the upper intercept may reflect some combination of laboratory and geologically meaningful trapped initial lead (Xiang *et al.* 2021). Additional Pb mixing components, dependent

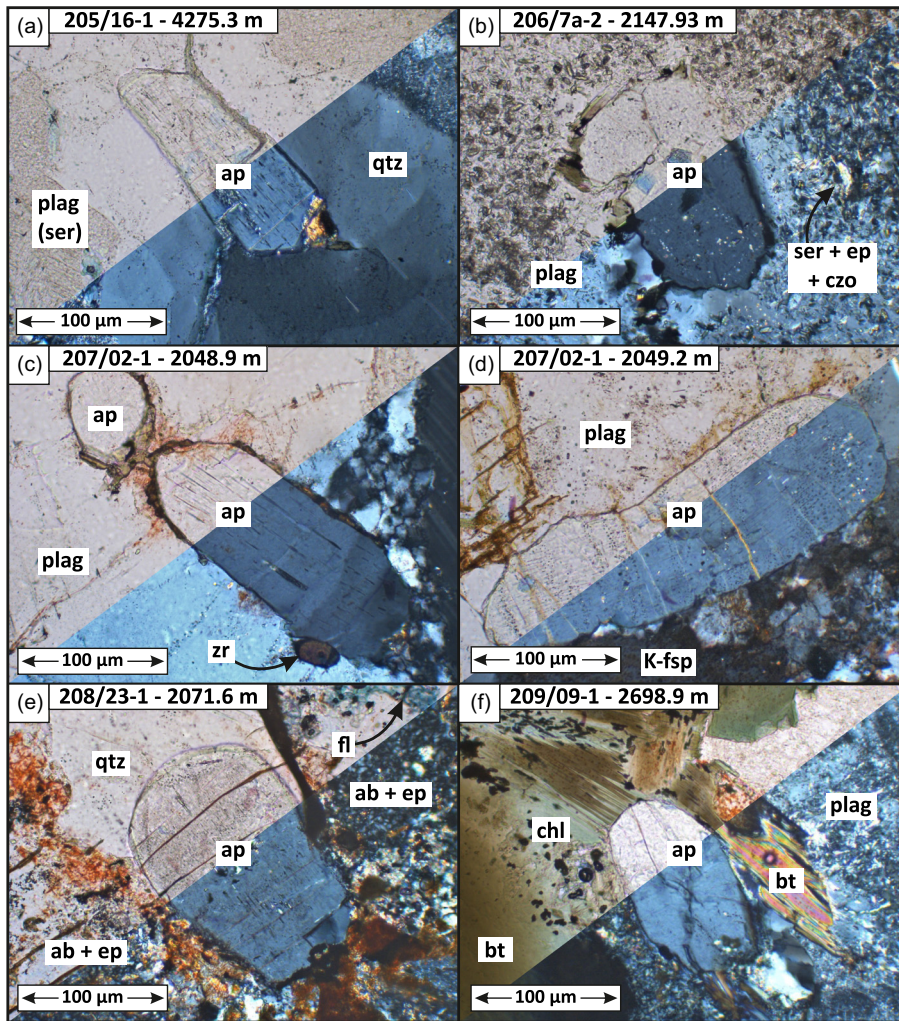


**Fig. 4.** Thin-section photomicrographs showing the typical form and internal structure of apatite exhibited in samples collected within each well except 208/27-2. All photomicrographs comprise a PPL and XPL montage. (a) Subhedral prismatic apatite enclosed in quartz (205/16-1, 4275.3 m). (b) Anhedra to subhedral apatite hosting numerous fluid inclusions, enclosed within altered plagioclase (206/7a-2, 2147.93 m). (c) Euhedral to subhedral equant (top left) and prismatic (central) apatite enclosed within plagioclase (207/02-1, 2048.9 m). (d) Subhedral prismatic apatite hosting numerous fluid inclusions and intragranular fractures, situated along a plagioclase–K-feldspar grain boundary (207/02-1, 2049.2 m). (e) Rounded to subhedral apatite hosting fluid inclusions and numerous intragranular fractures situated along a quartz–plagioclase (albitized) grain boundary (208/23-1, 2071.6 m). (f) Subhedral prismatic apatite displaying several intragranular fractures enclosed within plagioclase and bordered with chloritized biotite (209/09-1, 2698.9 m). ab, albite; ap, apatite; bt, biotite; chl, chlorite; czo, clinozoisite; ep, epidote; fl, fluorite; K-fsp, K-feldspar; plag, plagioclase; qtz, quartz; ser, sericite; zr, zircon.

on their composition, would cause deflections away from a single mixing line and may be caused by the ablation of inclusions, the loss (or gain) of radiogenic Pb, or a grain-specific differential closure to radiogenic Pb mobility, or indeed infrequently see loss (or gain) of U (Kirkland *et al.* 2018a). Such issues are of direct concern in laser ablation studies, which may not directly measure  $^{204}\text{Pb}$ , and thus are unable to utilize a traditional 204 common Pb correction. Rather, laser ablation benefits from high data throughput that may allow better resolution of Pb mixing lines and the application of 207 correction (Chew *et al.* 2014). Such laser approaches have led to the realization that for common Pb-bearing minerals (e.g. apatite, titanite, etc.) the assumption of a terrestrial Pb model may lead to (grossly) inaccurate geochronology, necessitating direct knowledge on the trapped common Pb composition (Storey *et al.* 2006). In brief, 207 correction projects a mixing line from an assumed common Pb composition through the measured Pb isotopic ratios onto the concordia, which defines in essence a model age (Williams 1998). Hence, a further obvious complication is the choice of common Pb in the calculation of any apparent age for any individual apatite analyses (which could be most important in the case of detrital studies where a common source fluid growing the apatite was unlikely).

There are two ways in which this problem can be approached, each associated with some arbitrary assumptions. The trapped common Pb composition can be estimated based on an iterative approach (Model 1) assuming a Pb model composition (e.g. Stacey and Kramers 1975). Such an approach starts by assuming some nominal Pb<sub>0</sub> composition (e.g. 0.83 modern Pb) and calculates a 207 corrected age based on this. The common Pb composition is then

remodelled based on this preliminary 207 corrected age, using some favoured Pb evolution model. This calculation process continues, recalculating a new common Pb model value from the preliminary 207 corrected age and so on, until no subsequent change in 207 corrected age occurs (Chew *et al.* 2011). In effect, this is a line balancing approach, which may work well for samples with U (low common Pb) but is forced to make some unpalatable arbitrary assumptions related to the composition of common Pb that can be especially problematic for low U analyses. The effect of this strategy is to use those more radiogenic analyses to weight themselves more towards a potentially more appropriate model common Pb composition (because their age is arguably better constrained), whereas those with higher common Pb composition are, by necessity, weighted more towards the starting common Pb assumption as a function of having less information to pick the appropriate time for the common Pb model. This approach essentially brings greater information into the choice of common Pb than picking, for example, a static modern value for the calculation.

Nonetheless, it is clear that in many samples mixing lines between the common and radiogenic component can be well defined, pointing towards a singular ordinate intercept on inverse concordia plots. Hence, the alternative approach (Model 2) describes the common Pb based on a regression through the data in Tera and Wasserburg space, with the upper intercept specifically defining the common Pb composition. This is an important unique advantage of the Model 2 207 correction approach, as it is not forced to use a Pb model in the estimation of this value (in contrast to the typical application of a 204 correction, for example). Goodness of

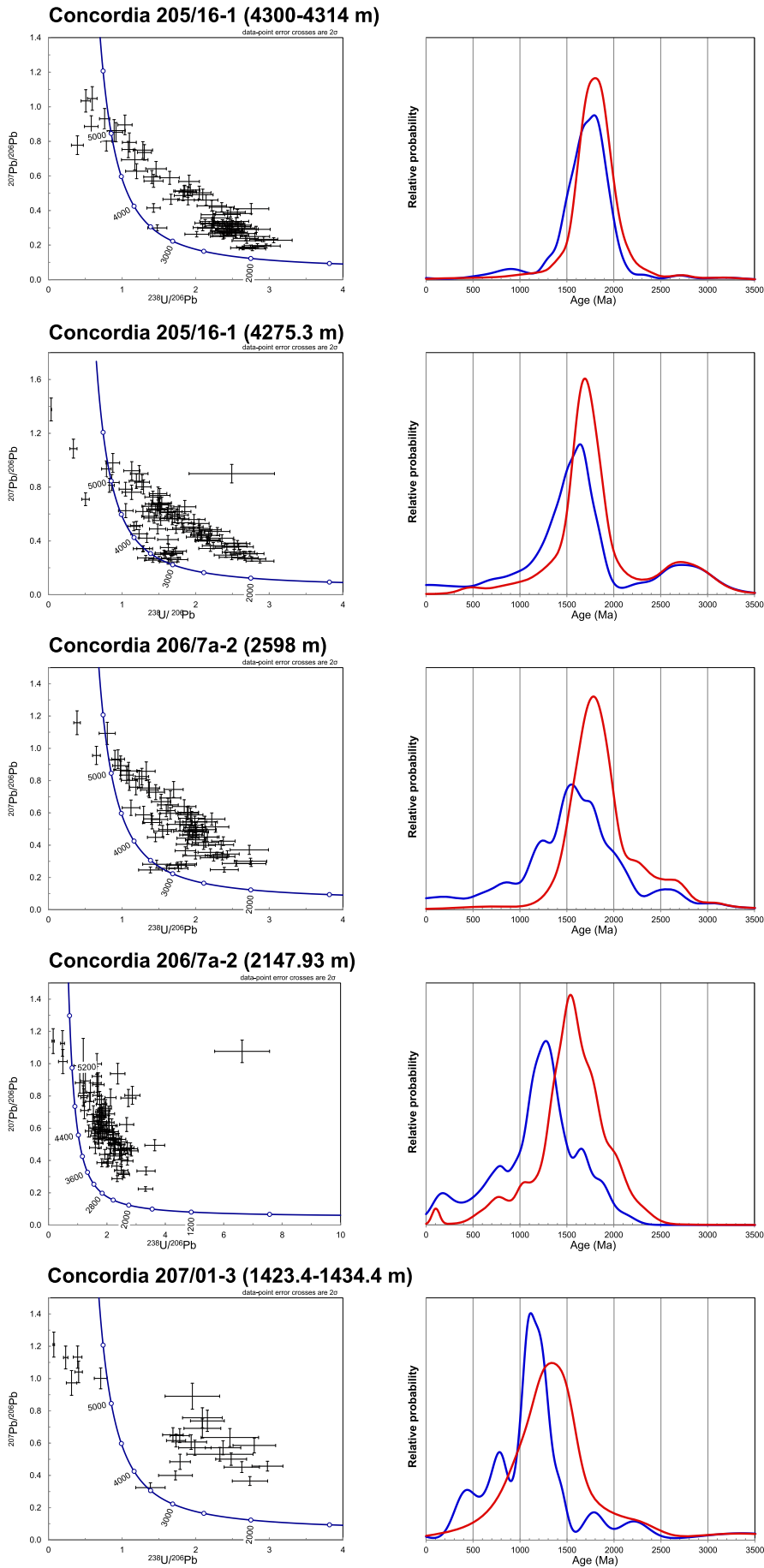


**Fig. 5.** Concordia and probability density plots for each of the analysed samples ( $2\sigma$  uncertainties). These are ordered on a geographical basis, south to north. The blue and red curves in the probability density plots correspond, respectively, to the Model 1 and 2 calculation approaches.

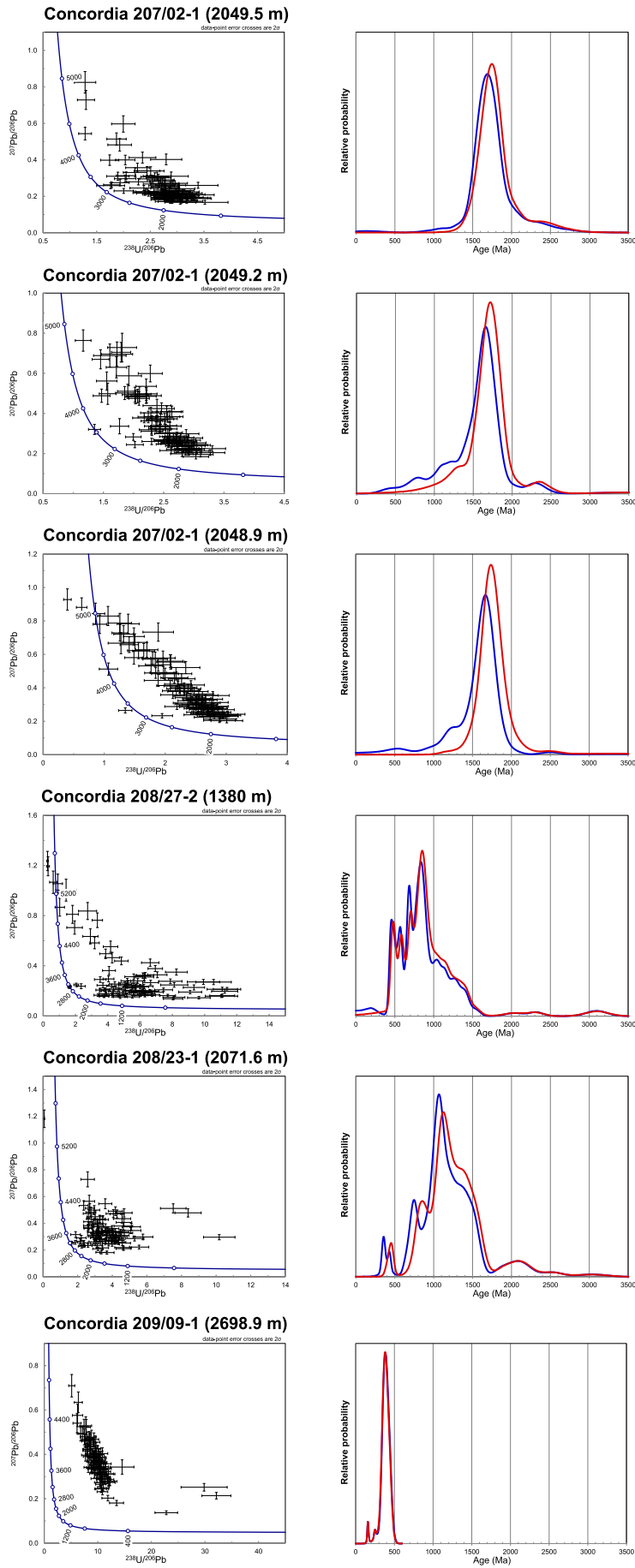


Fig. 5. Continued.

fit parameters to this regression inform on the suitability of the common Pb, which is defined by the data and not a model. However, when there is complexity in the dataset, as would be expected for grains that closed to Pb diffusion at different times or grew from different source fluids, this approach will struggle to uniquely define the common Pb component.

Here we apply both approaches. We assess 207 corrected ages from Model 1 and use these to help group (age) coherent analyses that apparently define sets of coherent U–Pb ratios to apply the Model 2 solution (e.g. fitting regressions to define the common Pb component). Specifically, we select those ratios for Model 1 ages within the 20–80 percentile for regression on a per sample basis. More, restrictive grouping could be applied and further subsets selected to define additional common Pb values, but this has little implication for the dataset under consideration here (owing to the distribution of values around generally well-defined mixing lines), but may be useful elsewhere. In any case, the grouped data defined regressions provide new common Pb values that can be applied to each measured ratio pair. Thus, the new common Pb value (and error) is used in subsequent 207 corrected age calculations (Model 2 ages). In this way we are able to select common Pb values per sample, which best resolves the trapped common Pb value for the majority of that sample's analyses.

We suggest a mechanism to select the most appropriate choice between Model 1 and Model 2 ages, which ultimately comes down to how well the data define a singular mixing line v. scatter (as could be expected for multiple growth events or various closure temperatures recorded within a sample).

## Results

The results for each sample are presented as concordia and probability density plots (Fig. 5), which are ordered on a geographical basis, south to north. The probability density plots each contain blue and red curves, which correspond, respectively, to the Model 1 and 2 calculation approaches outlined above. Each sample displays a dominant age peak, and a number displays one or more subsidiary age peaks as tabulated in Table 1.

## Discussion

### A vexing question, the choice of common Pb

In addition to simply evaluating the distribution of data on inverse concordia plots, one additional mechanism to assist in picking the most appropriate model (Model 1 or 2) for common Pb correction may be by comparing plots of 207 corrected age v. F207% (Fig. 6). F207% is the percentage of common Pb as estimated by the amount of discordance along a mixing line towards the defined or modelled

common Pb composition from the measured ratio (Kirkland *et al.* 2018a):

$$\begin{aligned} & \text{Concordant } ^{206}\text{Pb}/^{238}\text{U} \text{ ratio} \\ &= \text{EXP}(0.000155125 \times 207 \text{ corrected } ^{238}\text{U}/^{206}\text{Pb} \text{ age}) - 1 \\ & \text{F207\%} \\ &= 100 \times (1 - \text{Concordant } ^{206}\text{Pb}/^{238}\text{U} \text{ ratio}/^{206}\text{Pb}/^{238}\text{U} \text{ measured}) \end{aligned}$$

Such plots for Model 1 data reveal a curved array through a dominant *c.* 1700 Ma component. If interpreted as geologically meaningful this pattern would imply more common Pb associated with more Pb loss or recrystallization, following a power-law relationship. It is questionable whether apatite would geologically respond in such fashion. However, this pattern in age v. F207 could also simply be a function of apparently younger (e.g. recrystallized) apatite calculated in the Model 1 approach having a predicted common Pb value that was too low (unradiogenic), a direct function of how common Pb was estimated via iteration using a Pb evolution model. In contrast, a plot of the same data using a static common Pb value (e.g. Model 2) produces less of a slope (e.g. more discrete grouping) between F207 and apparent age (207 corrected), supporting the interpretation that Model 2 ages better capture an appropriate common Pb value for more of the analyses.

The 400 Ma apparent age component also displays a slight skew to higher common Pb (F207) for younger ages when Pb<sub>i</sub> is estimated using an iterative approach, consistent with more common Pb in apatite that has apparently younger ages, or a systematic underestimation of Pb<sub>i</sub> for these analyses. When using a static Pb<sub>i</sub> value for common lead skewness between 207 corrected age components and common Pb content is reduced, again arguably supporting the latter interpretation; namely, an underestimation of the Pb<sub>i</sub> ratio using a Model 1 approach.

Ultimately, this comparison highlights that the source from which some of the samples have been sourced has a higher <sup>207</sup>Pb/<sup>206</sup>Pb ratio than the Stacey and Kramers (1975) terrestrial Pb evolution model. More specifically, this implies that the crust from which this apatite (re)grew was more U enriched than the terrestrial average. Furthermore, in all cases lower apparent ages with lower F207 are the most robust as they require less estimation of common Pb and yield apparent ages that are similar between the different correction methods.

### U–Pb apatite record and correlations with tectonic events; evidence for widespread isotopic resetting

The major and minor peaks in the probability density plots (Table 1; Figs 5 and 7) can be divided into six broad age groups, each of which temporally overlaps a major tectonic or magmatic event recorded in one or more of the Lewisian Gneiss Complex to the south, the Faroe–Shetland terrane itself and the Caledonides of northern Scotland to the east (Table 2), as follows.

- (1) Group 1. Neoproterozoic apatite age peaks of *c.* 2750, *c.* 2700 and *c.* 2600 Ma are close to the U–Pb zircon crystallization protolith ages obtained from the FST orthogneisses in all but one (209/09-1) of the samples. Mineralogical and textural evidence for early upper amphibolite- to granulite-facies metamorphism within the FST (Chambers *et al.* 2005; Holdsworth *et al.* 2019) is supported by the present study. However, previous studies did not explicitly address the question of when this occurred. The published U–Pb zircon ages from the FST basement were all obtained from the cores of zircon grains that were interpreted to be igneous in origin. Furthermore, there is no evidence on concordia diagrams for anything other than modest radiogenic Pb loss, much of which may have occurred during sedimentation of

**Table 1.** Summary of the main and subsidiary age peaks displayed in the density distribution plots (Fig. 5)

Well number (and depth)	Dominant and subsidiary age peaks (Ma)*
205/16-1 (4300–4314 m)	1800
205/16-1 (4275.3 m)	1700, 2750
206/7a-2 (2598 m)	1600, 2600, 1250
206/7a-2 (2147.93 m)	1300, 1700, 800, 200
207/01-3 (1423.4–1434.4 m)	1100, 2700, 1800, 800, 450
207/02-1 (2048.9, 2049.2, 2049.5 m)	1700
208/27-2 (1380 m)	800, 700, 600, 450
208/23-1 (2071.6 m)	1100, 800, 400, 350
209/09-1 (2698.9 m)	400

\*Dominant age peak is first value in each entry; subsidiary age peaks are following values.

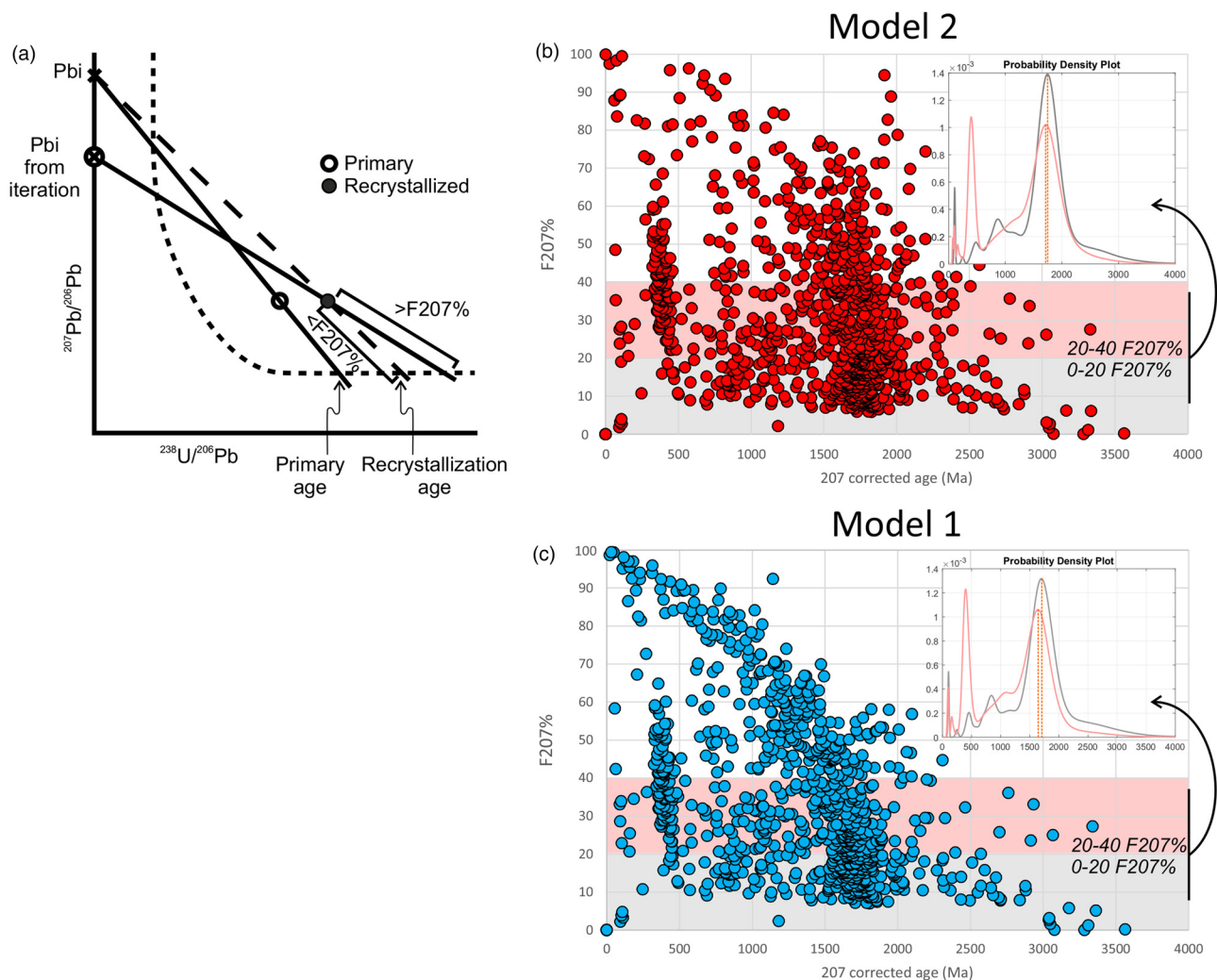


**Fig. 6.** (a) Schematic representation of a Tera and Wasserburg concordia plot with mixing lines between common and radiogenic components. The plot illustrates that as common  $^{207}\text{Pb}/^{206}\text{Pb}$  ( $\text{Pb}_i$ ) becomes more radiogenic (higher value) so F207% will decrease. (b) F207% v. 207 corrected apparent age based on Model 2 common Pb correction. (c) F207% v. 207 corrected apparent age based on Model 1 common Pb correction. Comparison of 207 corrected apparent ages for lower (grey fill, black line) versus higher (red fill, red line) common Pb content analyses is shown in the inset probability density diagrams for both models.

overlying Mesozoic successions (Holdsworth *et al.* 2019). We therefore conclude that the most likely scenario is that emplacement of the igneous protoliths and high-temperature metamorphism were contemporaneous Neoproterozoic events. The igneous protoliths were probably emplaced into a deep crustal environment at upper amphibolite- to granulite-facies conditions. The Neoproterozoic peaks recorded in the apatite data therefore probably correspond to the Neoproterozoic magmatic–metamorphic event.

- (2) Group 2. Late Neoproterozoic apatite peaks of *c.* 1800, *c.* 1700 and *c.* 1600 Ma overlap the timing of major magmatic and metamorphic events within the Lewisian Gneiss Complex on the Scottish mainland. These include high-grade Laxfordian metamorphism and associated deformation at 1880–1740 Ma (Friend and Kinny 2001; Volante *et al.* 2023) and syntectonic granitic pegmatite emplacement at *c.* 1790–1770 Ma in the vicinity of the Laxford Shear Zone (Goodenough *et al.* 2013), as well as lower-grade reworking and shear zone development at 1690–1670 Ma (Corfu *et al.* 1994; Friend and Kinny 2001). Offshore and close to the inferred northern ‘front’ of Nagssugtoqidian reworking (Fig. 1), a U–Pb zircon age of  $1634 \pm 3$  Ma was obtained for the igneous protolith of a granulite-facies mafic gneiss sampled in exploration well

164/25-2 (Chambers *et al.* 2005), and preliminary U–Pb titanite ages of *c.* 1710–1650 Ma are reported from Sula Sgeir (Fig. 2; Goodenough *et al.* 2024). High-temperature reworking at *c.* 1700–1600 Ma also affected the Neoproterozoic basement inliers east of the Moine Thrust (Imber *et al.* 2002; Bird *et al.* 2023).

- (3) Group 3. Late Mesoproterozoic apatite peaks of *c.* 1300, *c.* 1250 and *c.* 1100 Ma are coeval with accretionary orogenesis outboard of Laurentia and its subsequent collision with Baltica to create a short northern arm of the Grenville orogen (Strachan *et al.* 2020b). In Scotland these events are recorded within the Lewisian Gneiss Complex by early ductile thrusting along the Outer Hebrides Thrust (*c.* 1100–1000 Ma, U–Pb apatite; Metcalfe *et al.* 2024), and within the Caledonides by eclogite-facies metamorphism of the Eastern Glenelg basement inlier (*c.* 1200 Ma, Lu–Hf garnet; Bird *et al.* 2023), and upper amphibolite-facies metamorphism of the Cullivoe basement inlier in Shetland (*c.* 1050 Ma, Lu–Hf garnet; Walker *et al.* 2021).
- (4) Group 4. Neoproterozoic apatite peaks of *c.* 800, 700 and 600 Ma overlap a number of tectonic events. The *c.* 800 Ma peak broadly corresponds to Knoydartian orogenic events recognized within the Caledonides (Rogers *et al.* 1998; Vance *et al.* 1998; Cutts *et al.* 2010; Cawood *et al.* 2015).

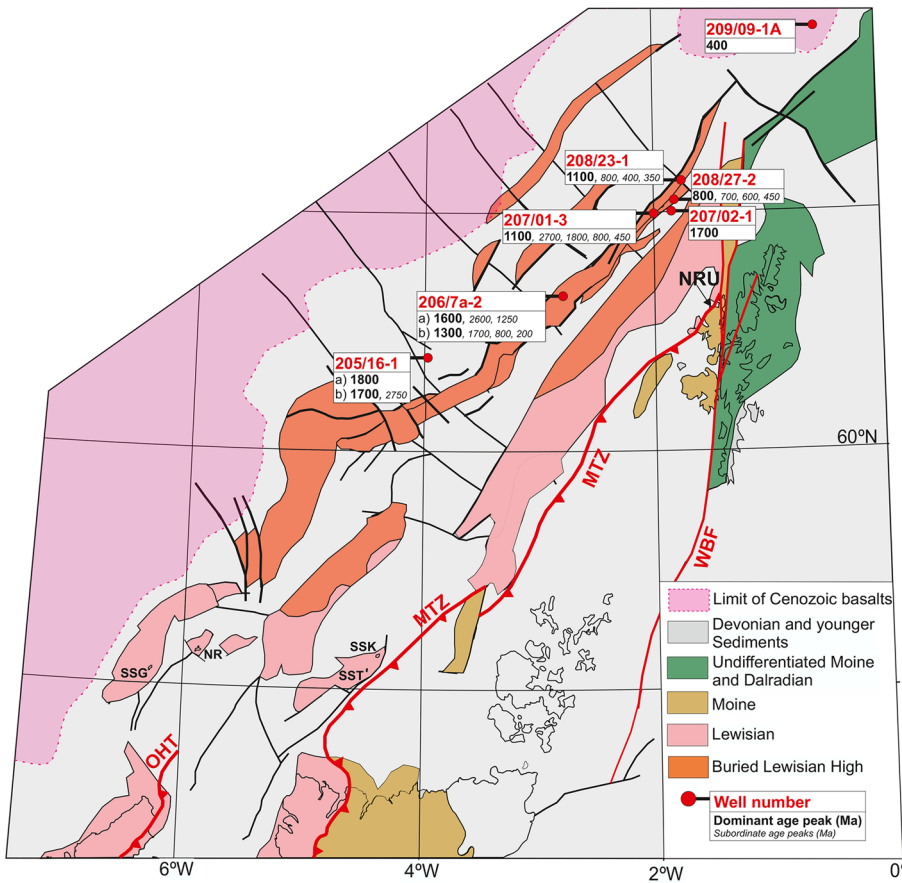


Fig. 7. Map based on Figure 2, showing the U–Pb apatite age peaks in the samples from the seven wells studied.

Table 2. Comparison of the apatite ages reported here and regional-scale tectonothermal events recorded within the Lewisian Gneiss Complex, Faroe–Shetland terrane and the northern Scottish Caledonides

Lewisian Gneiss Complex (Hebridean terrane; HT)	Faroe–Shetland terrane (FST)	Northern Scotland Caledonides (NSC east of Moine Thrust Zone)	Apatite age peaks in FST
Neoarchaean: 3000–2500 Ma: emplacement of igneous protoliths into lower crustal environment; granulite- to amphibolite-facies metamorphism in HT (Badcallian and Inverian events) and FST; NSC metamorphic grade not documented.			2750 Ma (205/16-1, 4275.3 m) 2700 Ma (207-01) 2600 Ma (206/7a-2, 2598 m)
Early Paleoproterozoic: 2418–2375 Ma: intrusion of Scourie dyke swarm	Not documented	Not documented	
Mid–Late Paleoproterozoic: 1900 Ma: crustal additions (e.g. Loch Maree Group); 1880–1740 Ma: Laxfordian granulite- to amphibolite-facies metamorphism and deformation; 1690–1670 Ma shear zones and lower-grade metamorphism	Not documented	1770–1655 Ma: crustal additions (e.g. Loch Shin inlier); 1700–1600 Ma: eclogite- (Glenelg inlier) and granulite(?) -facies (Borgie inlier) metamorphism	1800 Ma* (205/16-1, 4300–4314 m) 1700 Ma* (205/16-1, 4275.3 m) 1800 Ma (207-01) 1700 Ma (206/7a-2, 2147.93 m) 1700 Ma* (207/02-1) 1600 Ma* (206/7a-2, 2598 m)
Late Mesoproterozoic: 1300(?)–1000 Ma: Grenville orogeny, localized ductile thrusting (OHT)	Localized ductile thrusting?	Eclogite- (Glenelg) and amphibolite-facies (Shetland) metamorphism	1300 Ma* (206/7a-2, 2147.93 m) 1250 Ma (206/7a-2, 2598 m) 1100 Ma* (207-01) 1100 Ma* (208/23-1)
Not documented	Localized ductile thrusting?	Tonian: 950–930 Ma (Renlandian) and 840–725 Ma (Knoydartian) orogenic events	800 Ma (206/7a-2, 2147.93 m) 800 Ma (207-01) 800 Ma* (208/27-2) 800 Ma (208/23-1)
Not documented	Not documented	Cryogenian–Ediacaran: 700–565 Ma, Rodinia break-up, magmatism and opening of Iapetus Ocean	700 Ma (208/27-2) 600 Ma (208/27-2)
Margins affected within the Moine Thrust Zone	Margins affected within the northern continuation of the Moine Thrust Zone (Uyea Shear Zone; Kinny <i>et al.</i> 2019)	Ordovician–Silurian: 490–420 Ma, Caledonian orogeny, regional deformation and amphibolite-facies metamorphism	500 Ma (208/27-2) 450 Ma (207-01) 400 Ma (208/23-1) 400 Ma* (209/09-1)
Devonian–Carboniferous: post-Caledonian extension and sedimentary basin development			350 Ma (208/23-1)
Triassic–Jurassic boundary: onset of proto-NE Atlantic rifting?			200 Ma (206/7a-2)

\*Dominant age; other values are subsidiary age peaks.

The peaks of *c.* 700 and *c.* 600 Ma overlap, respectively, the likely initiation of the Dalradian sedimentary basin (*c.* 700 Ma?) and development of the Central Iapetan Magmatic Province during continental break-up and birth of the Iapetus Ocean (*c.* 600 Ma; Tegner *et al.* 2019).

- (5) Group 5. Early Paleozoic apatite peaks of *c.* 450 (Late Ordovician) and *c.* 400 Ma (Early Devonian) could correspond, respectively, to Grampian and Scandian phases of the Caledonian orogeny, or both could be accommodated within a protracted Scandian event (Bird *et al.* 2013; Law *et al.* 2024; Leslie 2024). The upper limit of Caledonian marginal thrusting is poorly constrained in NW Scotland (Strachan *et al.* 2020a), and along the strike of the orogen in East Greenland significant crustal thickening continued until at least 400–390 Ma (Dallmeyer *et al.* 1994; Gilotti *et al.* 2008).
- (6) Group 6. This comprises only two apatite age peaks of *c.* 350 and 200 Ma, both of which correspond to periods of basin development. The Caledonian orogeny was followed both onshore and offshore by Devonian–Carboniferous crustal extension, which overlaps the *c.* 350 Ma peak. Renewed extension in the latest Triassic to early Jurassic marks the onset of development of the proto-North Atlantic Ocean and overlaps the *c.* 200 Ma peak.

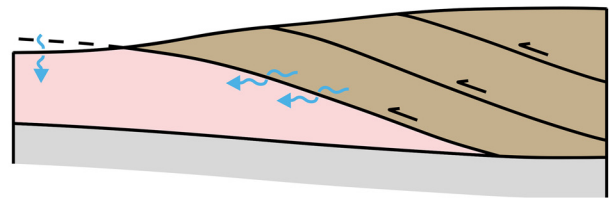
### Potential explanations for the overlaps between the apatite peaks and regional tectonic events

In a few cases, the significance of the apatite peaks is clear. As discussed, the Neoproterozoic peaks probably reflect cooling following plutonism and high-grade metamorphism through the Pb blocking temperature for apatite (375–550°C; Chew and Spikings 2015). At the opposite end of the age spectrum, the 400 Ma apatite age peak in well 209/09-1 (Fig. 5) was obtained east of the Moine Thrust from an Ordovician granitic orthogneiss (Fig. 7) and is most easily interpreted as representing the time at which the sample cooled following Caledonian metamorphism. These peaks need not be considered further. The interpretation of the remaining apatite data is less straightforward, and we cannot rule out the possibility that some minor age peaks in part reflect data obtained from apatite grains that were not age homogeneous. In all cases, the protolith lithologies are Neoproterozoic orthogneisses and the apatite grains are interpreted as part of the primary magmatic mineralogy (Figs 3 and 4). These samples show no evidence for any widespread high-temperature reworking. The Paleoproterozoic to Early Paleozoic age peaks that they exhibit must therefore reflect younger isotopic disturbances (resetting) of U–Pb systems. The close correlation of the apatite age peaks with tectonic events in adjacent crustal blocks leads to discussion of the potential drivers by which U–Pb resetting in apatite might have been achieved: (1) resetting by hot fluids expelled from these orogens during foreland-directed thrusting; (2) synmetamorphic ductile thrusting; (3) burial and static heating underneath thrust sheets that have subsequently been removed by erosion ('top down'); (4) heating consequent on late- to post-orogenic delamination ('bottom up'); (5) heating that accompanied crustal extension and basin development (Fig. 8).

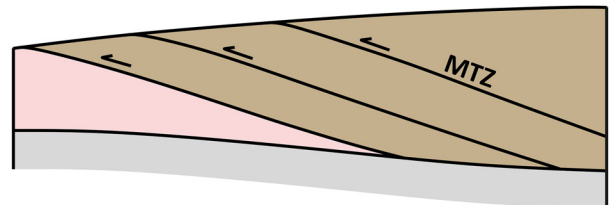
#### Could apatite have been reset by hot fluids?

Isotopic resetting of the U–Pb system in apatite by hot fluids might be expected to result in secondary recrystallization (Fig. 8a), but there is no textural indication of this in either petrographic thin sections or BSE images of the analysed grains. Any circulating hot fluids might also cause alteration of zircon crystals and Pb loss. For example, Larsen and Tullborg (1998) interpreted extensive Pb loss from zircons in Proterozoic basement gneisses in the Baltic Shield

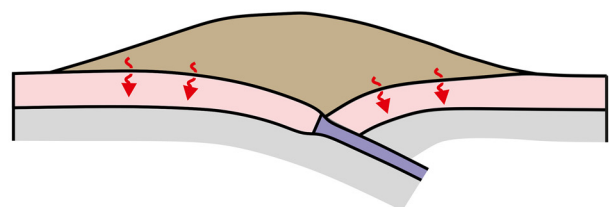
(a) Hot fluids flushed from orogen



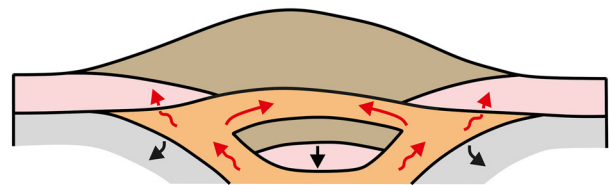
(b) Ductile thrusting



(c) "Top down" heating from the orogenic wedge



(d) "Bottom up" heating following delamination



(e) "Bottom up" heating during lithospheric extension

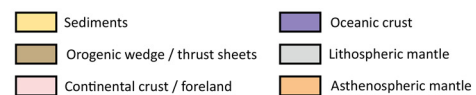
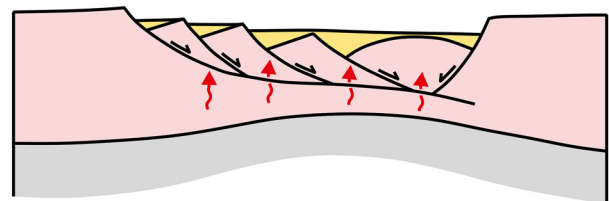


Fig. 8. Schematic representations of the potential mechanisms for isotopic resetting as discussed in the text. MTZ, Moine Thrust Zone.

to be the result of leaching by low-temperature hydrothermal solutions derived from Upper Paleozoic sedimentary rocks. Morris *et al.* (2015) demonstrated extensive Pb loss and development of metamict textures in detrital zircons within the foreland basin of the Caledonides in northern East Greenland, which they attributed to post-depositional fluid movement during the Middle Devonian. Within the FST, zircon grains appear to be unaltered, and the only Pb loss evident is most probably associated with Phanerozoic basin development (Holdsworth *et al.* 2019). Hence, it seems unlikely that hot fluids were the primary mechanism by which apatite U–Pb system was reset.

### Could the apatite ages record synmetamorphic ductile thrusting?

The pre-Mesozoic offshore geology is inevitably poorly understood and the currently defined limits of the FST may be imprecise. Both the ‘Moine Thrust’ defined in NW Shetland (Walker *et al.* 2016; Kinny *et al.* 2019) and the Nagsugtoqidian front could be the roof structures of ductile thrust zones that extend some distance offshore to the west and north respectively and enclose lozenges of Neoproterozoic basement that were reheated during thrusting (Fig. 8b depicts this scenario with reference to the Caledonian front). Knoydartian-age thrusts have not been reported from west of the Moine Thrust on the Scottish mainland, but there is no reason why this should be the case within the FST. A Grenvillian-age ductile thrust analogous to the Outer Hebrides Thrust (OHT) might extend along-strike NE into the area west and north of Shetland. Temperatures both within and in the footwall of the OHT were sufficient to reset apatite (Metcalf *et al.* 2024). The locally extensive networks of cataclasite and associated pseudotachylyte seen in some wells (Holdsworth *et al.* 2020, fig. 5e–g) may be related to such deformation events. It may be significant that samples from wells 207/01-3, 207/02-1 and 208/23-1, both within 30 km of the probable offshore location of the Moine Thrust, record evidence for grain-size reduction and recrystallization. This is most notable in well 207/01-3 at a structural level *c.* 30 m above the dated sample (Fig. 9a–d). The retrograde white mica–chlorite–carbonate-rich phyllonitic textures in this core are consistent with greenschist-facies mineral assemblages associated with both the Moine Thrust Zone mylonites in mainland Scotland (e.g. Holdsworth *et al.* 2007) and phyllonites associated with the Outer Hebrides Thrust (Imber *et al.* 2001). Although no wells are recorded as penetrating significant mylonite zones, deep seismic reflection profiles reveal east-dipping reflectors (of unknown age) in the footwall of the Moine Thrust that would reach seabed in the general vicinity of well 207/01-3 (Richie *et al.* 2011). It therefore seems possible that some combination of Grenvillian, Knoydartian and Caledonian thrusting could account for the Group 3, 4 and 5 apatite peaks.

### Could apatite have been reset by static ‘top down’ heating owing to burial beneath now-eroded thrust nappes?

Studies from the forelands of other orogens have assessed the impact of burial beneath thrust nappes (Fig. 8c). In the northernmost East

Greenland Caledonides, Rasmussen and Smith (2001) used conodont geothermometry to demonstrate an increase in tectonic overburden from 6.8 to 12.5 km over a horizontal distance of *c.* 50 km in a traverse from the foreland across parautochthonous strata towards the orogenic hinterland. In northern Scotland, Johnson *et al.* (1985) used illite crystallinity to estimate that temperatures owing to tectonic burial on the Caledonian foreland reached 250–300°C, equivalent to *c.* 10–12 km overburden for a distance of at least 30 km west of the Moine Thrust. In an <sup>40</sup>Ar/<sup>39</sup>Ar study of the Paleoproterozoic Cape Smith fold belt (Trans-Hudson orogen, Canada) and its footwall, Skipton *et al.* (2022) documented variably reset biotite ages within foreland basement. It was established that the pre-erosional thrust wedge extended at least *c.* 100 km beyond the present limit of the belt and imposed a widespread low-temperature (<300°C) and/or short-lived thermal overprint on foreland basement.

In the case of the FST, to reset U–Pb apatite systems would require significantly higher temperatures and hence greater overburden than any considered in the above case studies. The assumption for simplicity of a temperature in the middle of the 375–550°C range, and a geothermal gradient of *c.* 25°C km<sup>-1</sup>, results in a minimum overburden of *c.* 18 km. On the presumption that Group 2 apatites are associated with the Nagsugtoqidian–Laxfordian orogen, this overburden must have extended for at least 200 km north of the orogenic front (Fig. 1). Although information is limited, there is no indication from metamorphic assemblages or textures that the overburden increased to the south as would be expected in a traverse towards the orogenic core. It is therefore difficult to model an orogenic profile that compares with those that characterize other well-studied orogens (Pfiffner 2017 and references therein). For these reasons, static resetting owing to burial in the footwall of now eroded thrust nappes does not seem a viable mechanism to account for the Group 2 apatites. However, this thermal model cannot be ruled out as a potential mechanism to account for some of the younger peaks from groups 3–5, which are all located <30 km from the Moine Thrust (Fig. 7), particularly if the apatite blocking temperature was near the lower end of its typical range.

### Could apatite have been reset by static ‘bottom up’ heating during late- to post-orogenic delamination?

‘Bottom up’ heating was essentially invoked by Gillespie *et al.* (2022) to explain the widespread resetting of U–Pb apatite systems for *c.* 200 km south of the Nagsugtoqidian front in SW Greenland,

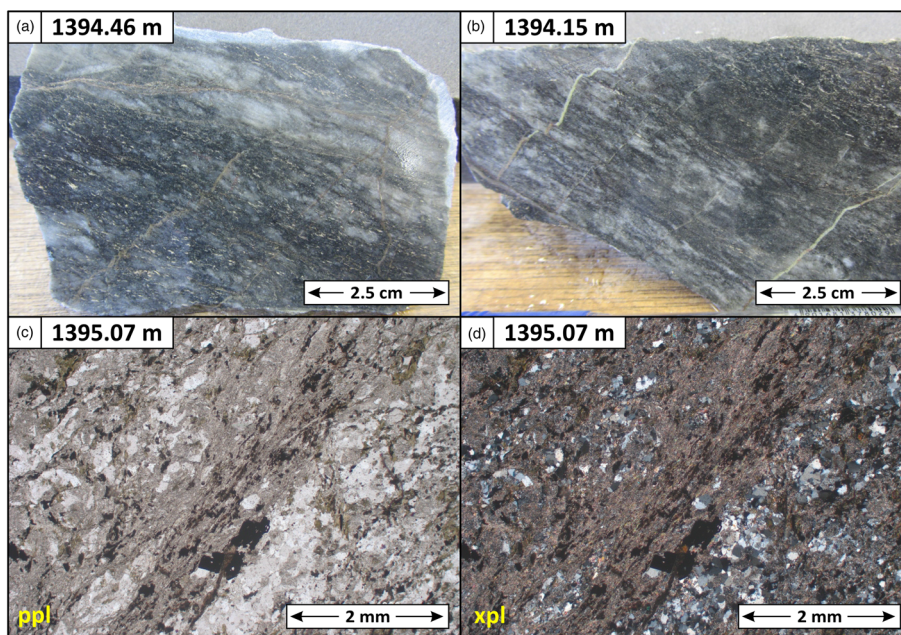


**Fig. 9.** Possible mylonitic–phyllonitic basement rocks from well 207/01-3, located *c.* 30 m above the sample dated in the present study. (a, b) Cut core samples showing strong tectonic fabric, relatively fine grain size and phyllosilicate enrichment relative to other basement cores. In (b) the cross-cutting fine epidote cataclasite veins locally offset across phyllosilicate layers should be noted. (c, d) Photomicrographs (ppl and xpl, respectively) showing mylonitic–phyllonitic textures, with significant enrichment in fine-grained white mica and chlorite. The localization of shear in phyllosilicate-rich domains should be noted.

a setting similar to that of the present study but on the opposite side of the orogen. Although it was not considered in detail, those workers suggested that heating associated with late orogenic collapse and extension generated a thermal anomaly that resulted in resetting of Neoproterozoic apatite grains. Late orogenic collapse typically results from delamination of the dense orogenic root, which sinks into the mantle to be replaced by hot asthenosphere, resulting in widespread melting of the upper mantle and/or the lower crust (Fig. 8d; Bird 1978, 1979; Li *et al.* 2016 and references therein). According to Kolb (2014), late-orogenic collapse of the Nagssugtoqidian orogen in SE Greenland occurred at *c.* 1740–1680 Ma, broadly overlapping the older U–Pb apatite age peaks within the FST. In SE Greenland, this was associated with the emplacement of post-tectonic diorites and granites in the orogenic hinterland. However, the results of numerical modelling predict that the thermal effects of delamination could extend for several hundred kilometres onto the forelands of collisional orogens (Ueda *et al.* 2012) and this seems a viable explanation for the Group 2 apatites. In principle, it could also account for Group 3, 4 and 5 apatites if repeated delamination followed Grenvillian, Knoydartian and Caledonian orogenies. A variant of delamination (slab break-off) has been widely applied to the Scottish Caledonides to explain late- to post-collisional magmatism (Atherton and Ghani 2002; Oliver *et al.* 2008; Neilson *et al.* 2009; Miles *et al.* 2016; Archibald *et al.* 2022; Milne *et al.* 2023).

#### Could apatite have been reset during high heat flux during continental extension?

The coincidence of 700 and 600 Ma peaks with periods of continental extension recognized within the Caledonides is a strong indication that the thermal effects of these events affected a large part of the Laurentian foreland (Fig. 8e; Tegner *et al.* 2019). It is notable that accessory minerals (monazite, xenotime, titanite and zircon) across a wide area of the northern Scottish Caledonides record evidence for resetting of U–Pb systems at *c.* 600 Ma, which has been attributed to static metamorphism or metasomatism related to high heat flux during continental rifting (Mako *et al.* 2021). The FST was itself the focus of extension during the Devonian–Carboniferous and the latest Triassic to Jurassic, hence enhanced heat flux during these episodes is the most likely explanation for the 350 and 200 Ma peaks.

## Conclusions

- (1) Plots of F207 v. 207 corrected ages provide a mechanism to evaluate the suitability of common Pb correction. On these plots, curvilinear patterns can imply calculation artefacts or natural processes that can be evaluated against *a priori* geological knowledge.
- (2) The Neoproterozoic foreland basement of the FST displays abundant evidence for isotopic resetting of U–Pb systems in apatite grains between *c.* 1800 and 200 Ma. There is no evidence that resetting was achieved by the flushing of hot fluids from adjacent orogens as invoked in other case studies, and it is more likely that episodic thermal pulses associated with regional-scale tectonic events were responsible.
- (3) Major age peaks of *c.* 1800–1600 Ma, which broadly correspond to the timing of Nagssugtoqidian–Laxfordian orogenesis, extend for at least 225 km north of the northern limit of Nagssugtoqidian–Laxfordian reworking. It is unrealistic to ascribe these to ‘top down’ heating beneath now-eroded thrust nappes; more plausibly they result from ‘bottom up’ heating during late- to post-orogenic delamination that affected a wide area of the orogenic foreland.

- (4) Late- to post-orogenic delamination might also account for major age peaks of *c.* 1300–1100, 800 and 500–400 Ma, corresponding to, respectively, Grenvillian, Knoydartian and Caledonian orogenic events. However, east-dipping seismic reflectors in the basement west of Shetland may represent the northward extension of the Grenvillian Outer Hebrides Thrust and/or Caledonian thrusts and so perturbation of isotherms during west-directed thrusting could therefore also account for these age peaks.
- (5) Minor age peaks of *c.* 700, 600, 350 and 200 Ma are most easily interpreted as resulting from enhanced heat flux that accompanied periods of crustal extension prior to and following the Caledonian orogeny.
- (6) The static lower to middle greenschist-facies retrogression that affected the Archean orthogneisses of the FST is most likely to result from one (or more) of the tectonic events associated with the major age peaks. Evidence for this retrogressive event is well developed as far west as well 205/16-1, which is dominated by Paleoproterozoic age peaks. It is therefore suggested that retrogression resulted from widespread heating following late- to post-Nagssugtoqidian–Laxfordian delamination.
- (7) Our study has widespread relevance to the study of other basement terranes as it highlights the importance of carrying out geochronological investigations of a wide range of minerals with different closure temperatures to clarify the complete thermal history, which might otherwise not be evident from petrographic studies.

*Scientific editing by Kathryn Cutts*

**Acknowledgements** The authors thank E. Dempsey for valuable discussions of the dataset and M. Witton for assistance in drafting. K. Cutts, D. Chew and A. Bird provided valuable review comments that clarified the text.

**Author contributions** RAS: conceptualization (equal), formal analysis (equal), investigation (lead), writing – original draft (lead), writing – review & editing (lead); CLK: conceptualization (equal), formal analysis (equal), investigation (equal), writing – original draft (supporting), writing – review & editing (supporting); AJF: conceptualization (equal), formal analysis (equal), investigation (equal), writing – original draft (equal), writing – review & editing (equal); DSW: conceptualization (supporting), formal analysis (supporting), investigation (supporting), writing – original draft (supporting), writing – review & editing (supporting); JHM: conceptualization (supporting), formal analysis (supporting), investigation (supporting), writing – original draft (supporting), writing – review & editing (supporting); REH: conceptualization (supporting), formal analysis (supporting), investigation (supporting), writing – original draft (supporting), writing – review & editing (supporting).

**Funding** This research received no specific grant from any funding agency in the public, commercial or not-for-profit sectors.

**Competing interests** The authors declare that they have no known competing financial interests or personal relationships that could have appeared to influence the work reported in this paper.

**Data availability** All data generated or analysed during this study are included in this published article and its [supplementary information files](#).

## References

- Archibald, D.B., Murphy, J.B., Fowler, M., Strachan, R.A. and Hildebrand, R.S. 2022. Testing petrogenetic models for contemporaneous mafic and felsic to intermediate magmatism with the ‘Newer Granite’ suite of the Scottish and Irish Caledonides. *Geological Society of America, Special Papers*, **554**, [https://doi.org/10.1130/2021.2554\(15\)](https://doi.org/10.1130/2021.2554(15))
- Atherton, M.P. and Ghani, A.A. 2002. Slab breakoff: a model for Caledonian, Late Granite syn-collisional magmatism in the orthotectonic (metamorphic) zone of Scotland and Donegal, Ireland. *Lithos*, **62**, 65–85, [https://doi.org/10.1016/S0024-4937\(02\)00111-1](https://doi.org/10.1016/S0024-4937(02)00111-1)

- Bird, P. 1978. Initiation of intracontinental subduction in the Himalaya. *Journal of Geophysical Research*, **85**, 4975–4987, <https://doi.org/10.1029/JB083iB10.p04975>
- Bird, P. 1979. Continental delamination and the Colorado Plateau. *Journal of Geophysical Research*, **84**, 7561–7571, <https://doi.org/10.1029/JB084iB13.p07561>
- Bird, A.F., Thirlwall, M.F. and Strachan, R.A. 2013. Lu–Hf and Sm–Nd dating of metamorphic garnet: evidence for multiple accretion events during the Caledonian orogeny in Scotland. *Journal of the Geological Society, London*, **170**, 301–317, <https://doi.org/10.1144/jgs2012-083>
- Bird, A.F., Cutts, K.A., Strachan, R.A., Thirlwall, M. and Hand, M. 2018. First evidence of Renlandian (c. 950 Ma) orogeny in Mainland Scotland: implications for circum-North Atlantic correlations and the status of the Moine Supergroup. *Precambrian Research*, **350**, 283–294, <https://doi.org/10.1016/j.precamres.2017.12.019>
- Bird, A., Thirlwall, M., Strachan, R.A., Miller, I., Dempsey, E. and Hardman, K. 2023. Eclogites and basement terrane tectonics in the northern arm of the Grenville orogen, NW Scotland. *Geoscience Frontiers*, **14**, 101668, <https://doi.org/10.1016/j.gsf.2023.101668>
- Cawood, P.A., Strachan, R.A., Cutts, K., Kinny, P.D., Hand, M. and Pisarevsky, S. 2010. Neoproterozoic orogeny along the margin of Rodinia: development of the Valhalla Orogen, North Atlantic. *Geology*, **38**, 99–102, <https://doi.org/10.1130/G30450.1>
- Cawood, P.A., Strachan, R.A. *et al.* 2015. Neoproterozoic to early Palaeozoic extension and contraction history of East Laurentian margin sequences: the Moine Supergroup, Scottish Caledonides. *Geological Society of America Bulletin*, **127**, 349–371, <https://doi.org/10.1130/B31068.1>
- Cawood, P.A., Strachan, R.A., Pisarevsky, S.A., Gladkochub, D.P. and Murphy, J.B. 2016. Linking collisional and accretionary orogenesis during Rodinia assembly and breakup: implications for models of supercontinent cycles. *Earth and Planetary Science Letters*, **440**, 118–126, <https://doi.org/10.1016/j.epsl.2016.05.049>
- Chambers, L., Derbyshire, F., Noble, S. and Ritchie, D. 2005. *NW UK Continental Margin: Chronology and Isotope Geochemistry*. British Geological Survey Commissioned Report, **CR/05/95**.
- Chemostrat 2014. Dating west of Shetland basement using U–Pb zircon ages: a reconnaissance study. Chemostrat, Welshpool.
- Chew, D.M. and Donelick, R.A. 2012. Combined Apatite Fission Track and U–Pb Dating by LA-ICP-MS and its Application in Apatite Provenance Analysis. *Mineralogical Association of Canada, Short Course*, **42**, 219–247.
- Chew, D.M. and Spikings, R.A. 2015. Geochronology and thermochronology using apatite: time and temperature, lower crust to surface. *Elements*, **11**, 189–194, <https://doi.org/10.2113/gselements.11.3.189>
- Chew, D. and Strachan, R.A. 2014. The Laurentian Caledonides of Scotland and Ireland. *Geological Society, London, Special Publications*, **390**, 45–91, <https://doi.org/10.1144/SP390.16>
- Chew, D.M., Sylvester, P.J. and Tubrett, M.N. 2011. U–Pb and Th–Pb dating of apatite by LA-ICP-MS. *Chemical Geology*, **280**, 200–216, <https://doi.org/10.1016/j.chemgeo.2010.11.010>
- Chew, D.M., Petrus, J.A. and Kamber, B.S. 2014. U–Pb LA-ICPMS dating using accessory mineral standards with variable common Pb. *Chemical Geology*, **363**, 185–199, <https://doi.org/10.1016/j.chemgeo.2013.11.006>
- Corfu, F., Heaman, L.M. and Rogers, G.R. 1994. Polymetamorphic evolution of the Lewisian complex, NW Scotland, as recorded by the U–Pb isotopic compositions of zircon, titanite and rutile. *Contributions to Mineralogy and Petrology*, **117**, 215–228, <https://doi.org/10.1007/BF00310864>
- Craw, D., Koons, P.O., Horton, T. and Chamberlain, C.P. 2002. Tectonically driven fluid flow and gold mineralisation in active collisional orogenic belts: comparison between New Zealand and western Himalaya. *Tectonophysics*, **348**, 134–153, [https://doi.org/10.1016/S0040-1951\(01\)00253-0](https://doi.org/10.1016/S0040-1951(01)00253-0)
- Crowley, Q.C., Key, R. and Noble, S.R. 2015. High-precision U–Pb dating of complex zircon from the Lewisian Gneiss Complex of Scotland using an incremental CA-ID-TIMS approach. *Gondwana Research*, **27**, 1381–1391, <https://doi.org/10.1016/j.gr.2014.04.001>
- Cutts, K.A., Hand, M., Kelsey, D.E., Wade, B., Strachan, R.A., Clark, C. and Netting, A. 2009. Evidence for 950–930 Ma metamorphism in the Shetland Islands, Scottish Caledonides: implications for early Neoproterozoic tectonics in the Laurentia–Baltica sector of Rodinia. *Journal of the Geological Society, London*, **166**, 1033–1047, <https://doi.org/10.1144/0016-76492009-006>
- Cutts, K.A., Kinny, P.D. *et al.* 2010. Three metamorphic events recorded in a single garnet: coupled phase modelling with in situ LA-ICPMS, and SIMS geochronology from the Moine Supergroup, NW Scotland. *Journal of Metamorphic Geology*, **28**, 249–267, <https://doi.org/10.1111/j.1525-1314.2009.00863.x>
- Dallmeyer, R.D., Strachan, R.A. and Henriksen, N. 1994. <sup>40</sup>Ar/<sup>39</sup>Ar mineral age record in NE Greenland: implications for tectonic evolution of the North Atlantic Caledonides. *Journal of the Geological Society, London*, **151**, 615–628, <https://doi.org/10.1144/gsjgs.151.4.0615>
- Davies, J.H.F.L. and Heaman, L.M. 2014. New U–Pb baddeleyite and zircon ages for the Scourie dyke swarm: a long-lived large igneous province with implications for the Palaeoproterozoic evolution of NW Scotland. *Precambrian Research*, **249**, 180–198, <https://doi.org/10.1016/j.precamres.2014.05.007>
- Dewey, J.F. and Strachan, R.A. 2003. Changing Silurian–Devonian relative plate motion in the Caledonides: sinistral transpression to sinistral transtension. *Journal of the Geological Society, London*, **160**, 219–229, <https://doi.org/10.1144/0016-764902-085>
- Evans, D.A.D. and Mitchell, R.N. 2011. Assembly and breakup of the core of Palaeoproterozoic–Mesoproterozoic supercontinent Nuna. *Geology*, **39**, 443–446, <https://doi.org/10.1130/G31654.1>
- Finlay, A.J., Wray, D.S., Comfort, G. and Moore, J.K. 2023. Radioactive Heat Production variations in the Faroe–Shetland Basin: key new heat production, geological and geochronological data for regional and local basin modelling. *Petroleum Geoscience*, **29**, <https://doi.org/10.1144/petgeo2022-039>
- Friend, C.R.L. and Kinny, P.D. 2001. A reappraisal of the Lewisian Gneiss Complex: geochronological evidence for its tectonic assembly from disparate terranes in the Proterozoic. *Contributions to Mineralogy and Petrology*, **142**, 198–218, <https://doi.org/10.1007/s004100100283>
- Friend, C.R.L., Strachan, R.A. and Kinny, P.D. 2008. U–Pb zircon dating of basement inliers within the Moine Supergroup, Scottish Caledonides: implications of Archaean protolith ages. *Journal of the Geological Society, London*, **165**, 807–815, <https://doi.org/10.1144/0016-76492007-125>
- Gillespie, J., Kirkland, C.L., Kinny, P.D., Simpson, A., Glorie, S. and Rankenburg, K. 2022. Lu–Hf, Sm–Nd, and U–Pb isotopic coupling and decoupling in apatite. *Geochemica et Cosmochimica Acta*, **338**, 121–135, <https://doi.org/10.1016/j.gca.2022.09.038>
- Gilotti, J.A., Jones, K.A. and Elvevold, S. 2008. Caledonian metamorphic patterns in Greenland. *Geological Society of America, Memoirs*, **202**, 201–225, [https://doi.org/10.1130/2008.1202\(08\)](https://doi.org/10.1130/2008.1202(08))
- Goodenough, K.M., Crowley, Q.C., Krabbendam, M. and Parry, S.F. 2013. New U–Pb age constraints for the Laxford Shear Zone, NW Scotland: evidence for tectonomagmatic processes associated with the formation of a Palaeoproterozoic supercontinent. *Precambrian Research*, **233**, 1–19, <https://doi.org/10.1016/j.precamres.2013.04.010>
- Goodenough, K.M., Guice, G.L., Bird, A.F., Dempsey, E.D., Hughes, H.S.R. and Johnson, T.E. 2024. The Archaean and Palaeoproterozoic rocks of Scotland. In: Smith, M. and Strachan, R.A. (eds) *The Geology of Scotland*, 5th edn. Geological Society, London, in press.
- Holdsworth, R.E., Alsop, G.I. and Strachan, R.A. 2007. Tectonic stratigraphy and structural continuity of the northernmost Moine Thrust Zone and Moine Nappe, Scottish Caledonides. *Geological Society, London, Special Publications*, **272**, 121–142, <https://doi.org/10.1144/GSL.SP.2007.272.01.08>
- Holdsworth, R.E., Morton, A. *et al.* 2019. The nature and significance of the Faroe–Shetland Terrane: linking Archaean basement blocks across the North Atlantic. *Precambrian Research*, **321**, <https://doi.org/10.1016/j.precamres.2018.12.004>
- Holdsworth, R.E., Trice, R. *et al.* 2020. The nature and age of basement host rocks and fissure fills in the Lancaster field fractured reservoir, West of Shetland. *Journal of the Geological Society, London*, **177**, 686–699, <https://doi.org/10.1144/jgs2020-011>
- Imber, J., Holdsworth, R.E., Butler, C.A. and Strachan, R.A. 2001. A reappraisal of the Sibson–Scholz fault zone model: the nature of the frictional to viscous ('brittle–ductile') transition along a long-lived crustal-scale fault, Outer Hebrides, Scotland. *Tectonics*, **20**, 601–624, <https://doi.org/10.1029/2000TC001250>
- Imber, J., Strachan, R.A., Holdsworth, R.E. and Butler, C.A. 2002. Evidence for post-Laxfordian (Grenville?) initiation of the Outer Hebrides Fault Zone. *Geological Magazine*, **139**, 609–619, <https://doi.org/10.1017/S0016756802006969>
- Johnson, M.R.W., Kelly, S.P., Oliver, G.J.H. and Winter, D.A. 1985. Thermal effects and timing of thrusting in the Moine thrust zone. *Journal of the Geological Society, London*, **142**, 863–874, <https://doi.org/10.1144/gsjgs.142.5.0863>
- Kalsbeek, F., Austrheim, H., Bridgwater, D., Hansen, B.T., Pedersen, S. and Taylor, P.N. 1993. Geochronology of Archaean and Proterozoic events in the Ammassalik area, South-East Greenland, and comparisons with the Lewisian of Scotland and the Nagssugtoqidian of West Greenland. *Precambrian Research*, **62**, 239–270, [https://doi.org/10.1016/0301-9268\(93\)90024-V](https://doi.org/10.1016/0301-9268(93)90024-V)
- Kelly, N.M., Hinton, R.W., Harley, S.L. and Appleby, S.K. 2008. New SIMS U–Pb zircon ages from the Langavat Belt, South Harris, NW Scotland: implications for the Lewisian terrane model. *Journal of the Geological Society, London*, **165**, 167–181, <https://doi.org/10.1144/0016-76492007-116>
- Kinny, P.D. and Friend, C.R.L. 1997. U–Pb isotopic evidence for the accretion of different crustal blocks to form the Lewisian Complex of northwest Scotland. *Contributions to Mineralogy and Petrology*, **129**, 326–340, <https://doi.org/10.1007/s004100050340>
- Kinny, P.D., Friend, C.R.L. and Love, G.J. 2005. Proposal for a terrane-based nomenclature for the Lewisian Gneiss Complex of NW Scotland. *Journal of the Geological Society, London*, **162**, 175–186, <https://doi.org/10.1144/0016-764903-149>
- Kinny, P.D., Strachan, R.A. *et al.* 2019. The Neoproterozoic Uyea Gneiss Complex, Shetland: an onshore fragment of the Rae Craton on the European Plate. *Journal of the Geological Society, London*, **176**, 847–862, <https://doi.org/10.1144/jgs2019-107>
- Kirkland, C.L., Fougereuse, D., Reddy, S.M., Hollis, J. and Saxey, D.W. 2018a. Assessing the mechanisms of common Pb incorporation into titanite. *Chemical Geology*, **483**, 558–566, <https://doi.org/10.1016/j.chemgeo.2018.03.026>
- Kirkland, C.L., Yakymchuk, C., Szilas, K., Evans, N., Hollis, J., McDonald, B. and Gardiner, N.J. 2018b. Apatite: a U–Pb thermochronometer or geochronometer? *Lithos*, **318–319**, 143–157, <https://doi.org/10.1016/j.lithos.2018.08.007>

- Kolb, J. 2014. Structure of the Palaeoproterozoic Nagssugtoqidian Orogen, South-East Greenland: model for the tectonic evolution. *Precambrian Research*, **255**, 809–822, <https://doi.org/10.1016/j.precamres.2013.12.015>
- Krabbendam, M., Strachan, R.A. and Prave, A.R. 2021. A new stratigraphic framework for the early Neoproterozoic successions of Scotland. *Journal of the Geological Society, London*, **178**, jgs2021-054, <https://doi.org/10.1144/jgs2021-054>
- Larsen, S.A. and Tullborg, E.L. 1998. Why Baltic Shield zircons yield late Palaeozoic, lower intercept ages on U–Pb concordia. *Geology*, **26**, 919–922, [https://doi.org/10.1130/0091-7613\(1998\)026<0919:WBSZYL>2.3.CO;2](https://doi.org/10.1130/0091-7613(1998)026<0919:WBSZYL>2.3.CO;2)
- Law, R.D., Strachan, R.A., Thirlwall, M. and Thigpen, J.R. 2024. The Caledonian orogeny: Late Ordovician to Early Devonian tectonic and magmatic events associated with closure of the Iapetus Ocean. In: Smith, M. and Strachan, R.A. (eds) *The Geology of Scotland*, 5th edn. Geological Society, London, in press.
- Leslie, A.G. 2024. Early to Middle Ordovician ophiolite obduction, Grampian orogenesis and arc–continent collision (c. 490–460 Ma). In: Smith, M. and Strachan, R.A. (eds) *The Geology of Scotland*, 5th edn. Geological Society, London, in press.
- Li, Z.-H., Liu, M. and Gerya, T.V. 2016. Lithospheric delamination in continental collision orogens: a systematic numerical study. *Journal of Geophysical Research: Solid Earth*, **121**, 5186–5211, <https://doi.org/10.1002/2016JB013106>
- Li, Z.X., Bogdanova, S.V. *et al.* 2008. Assembly, configuration, and break-up history of Rodinia: a synthesis. *Precambrian Research*, **160**, 179–210, <https://doi.org/10.1016/j.precamres.2007.04.021>
- Love, G.J., Kinny, P.D. and Friend, C.R.L. 2004. Timing of magmatism and metamorphism in the Grunard Bay area of the Lewisian Gneiss Complex: comparisons with the Assynt Terrane and implications for terrane accretion. *Contributions to Mineralogy and Petrology*, **146**, 620–636, <https://doi.org/10.1007/s00410-003-0519-1>
- Mako, C., Law, R.D. *et al.* 2021. Growth and fluid-assisted alteration of accessory phases before, during and after Rodinia breakup: U–Pb geochronology from the Moine Supergroup rocks of northern Scotland. *Precambrian Research*, **335**, 106089, <https://doi.org/10.1016/j.precamres.2020.106089>
- Mark, D.F., Parnell, J., Kelley, S.P. and Sherlock, S.C. 2007. Resolution of regional fluid flow related to successive orogenic events on the Laurentian margin. *Geology*, **35**, 547–550, <https://doi.org/10.1130/G23388A.1>
- Mason, A.J. 2012. Major early thrusting as a control on the Palaeoproterozoic evolution of the Lewisian Complex: evidence from the Outer Hebrides, NW Scotland. *Journal of the Geological Society, London*, **169**, 201–212, <https://doi.org/10.1144/0016-76492011-099>
- Mason, A.J. 2016. The Palaeoproterozoic anatomy of the Lewisian Complex, NW Scotland: evidence for two ‘Laxfordian’ tectonothermal cycles. *Journal of the Geological Society, London*, **173**, 153–169, <https://doi.org/10.1144/jgs2015-026>
- Metcalf, J., Strachan, R.A., Darling, J., Fowler, M.B., Chapman, G. and Dunlop, J. 2024. U–Pb geochronology and microstructural analysis of apatite within a Proterozoic mid-crustal shear zone, Outer Hebrides, Scotland. *Journal of the Geological Society, London*, **181**, jgs2023-139, <https://doi.org/10.1144/jgs2023-139>
- Miles, A.J., Woodcock, N.H. and Hawkesworth, C.J. 2016. Tectonic controls of post-subduction granite genesis and emplacement: the late Caledonian suite of Britain and Ireland. *Gondwana Research*, **39**, 250–260, <https://doi.org/10.1016/j.gr.2016.02.006>
- Milne, E.J.M., Neill, I. *et al.* 2023. Caledonian hot zone magmatism in the ‘Newer Granites’: insight from the Cluanie and Clunes plutons, Northern Scottish Highlands. *Journal of the Geological Society, London*, **180**, jgs2022-076, <https://doi.org/10.1144/jgs2022-076>
- Morris, G.A., Kirkland, C.L. and Pease, V. 2015. Orogenic palaeofluid flow revealed by discordant detrital zircons in the Caledonian foreland basin of northern Greenland. *Lithosphere*, **7**, 138–143, <https://doi.org/10.1130/L420.1>
- Neilson, J.C., Kokelaar, B.P. and Crowley, Q.G. 2009. Timing relations and cause of plutonic activity of the Siluro-Devonian post collision magmatic episode in the Grampian Terrane. *Journal of the Geological Society, London*, **162**, 741–744, <https://doi.org/10.1144/0016-76492008-069>
- Oliver, G.J.H., Wilde, S.A. and Wan, Y. 2008. Geochronology and geodynamics of Scottish granulites from the late Neoproterozoic break-up of Rodinia to Palaeozoic collision. *Journal of the Geological Society, London*, **165**, 661–674, <https://doi.org/10.1144/0016-76492007-105>
- Oliver, J. 1986. Fluids expelled tectonically from orogenic belts: their role in hydrocarbon migration and other geologic phenomena. *Geology*, **14**, 99–102, [https://doi.org/10.1130/0091-7613\(1986\)14<99:FETFOB>2.0.CO;2](https://doi.org/10.1130/0091-7613(1986)14<99:FETFOB>2.0.CO;2)
- Park, R.G. 2005. The Lewisian terrane model: a review. *Scottish Journal of Geology*, **41**, 105–118, <https://doi.org/10.1144/sjg41020105>
- Park, R.G. 2022. A regional explanation for Laxfordian tectonic evolution and its implications for the Lewisian terrane model. *Scottish Journal of Geology*, **58**, <https://doi.org/sjg2021-020>
- Passchier, C.W. and Trouw, R.A.J. 2005. *Microtectonics*, 2nd edn. Springer, Berlin.
- Pfiffner, O.A. 2017. Thick-skinned and thin-skinned tectonics: a global perspective. *Geosciences*, **7**, 71, [https://doi.org/10.1130/2006.2412\(09\)](https://doi.org/10.1130/2006.2412(09))
- Pickering, K.T., Bassett, M.G. and Siveter, D.J. 1988. Late Ordovician–Early Silurian destruction of the Iapetus Ocean: Newfoundland, British Isles and Scandinavia – a discussion. *Transactions of the Royal Society of Edinburgh: Earth Sciences*, **79**, 361–382, <https://doi.org/10.1017/S0263593300014358>
- Rasmussen, J.A. and Smith, M.P. 2001. Conodont geothermometry and tectonic overburden in the northernmost East Greenland Caledonides. *Geological Magazine*, **138**, 687–698, <https://doi.org/10.1017/S0016756801005908>
- Ritchie, J.D., Noble, D., Derbyshire, F., Millar, I. and Chambers, L. 2011. Pre-Devonian. BGS Research Report, **RR11/01**, 71–78.
- Rogers, G., Hyslop, E.K., Strachan, R.A., Paterson, B.A. and Holdsworth, R.E. 1998. The structural setting and U–Pb geochronology of Knoydartian pegmatites in W Inverness-shire: evidence for Neoproterozoic tectonothermal events in the Moine of NW Scotland. *Journal of the Geological Society, London*, **155**, 685–696, <https://doi.org/10.1144/gsjgs.155.4.0685>
- Rogers, J.J.W. and Santosh, M. 2002. Configuration of Columbia, a Mesoproterozoic Supercontinent. *Gondwana Research*, **5**, 5–22, [https://doi.org/10.1016/S1342-937X\(05\)70883-2](https://doi.org/10.1016/S1342-937X(05)70883-2)
- Sanders, I.S., Van Calsteren, P.W.C. and Hawkesworth, C.J. 1984. A Grenville Sm–Nd age for the Glenelg eclogite in northwest Scotland. *Nature*, **312**, 439–440, <https://doi.org/10.1038/312439a0>
- Skipton, D.R., St-Onge, M.R., Kellett, D.A., Joyce, N.L. and Smith, S. 2022. Rapid post-orogenic cooling of the Palaeoproterozoic Cape Smith foreland thrust belt and footwall Archaean basement, Trans-Hudson orogen, Canada. *Geological Society of America, Memoirs*, **220**, [https://doi.org/10.1130/2022.1220\(06\)](https://doi.org/10.1130/2022.1220(06))
- Soper, N.J., Strachan, R.A., Holdsworth, R.E., Gayer, R.A. and Greiling, R. 1992. Sinistral transpression and the Silurian closure of Iapetus. *Journal of the Geological Society, London*, **149**, 871–880, <https://doi.org/10.1144/gsjgs.149.6.0871>
- Stacey, J.S. and Kramers, J.D. 1975. Approximation of terrestrial lead isotope evolution by a two-stage model. *Earth and Planetary Science Letters*, **26**, 207–221, [https://doi.org/10.1016/0012-821X\(75\)90088-6](https://doi.org/10.1016/0012-821X(75)90088-6)
- Stipp, M., Stünitz, H., Heilbronner, R. and Schmid, S.M. 2002. Dynamic recrystallization of quartz: correlation between natural and experimental conditions. *Geological Society, London, Special Publications*, **200**, 171–190, <https://doi.org/10.1144/GSL.SP.2001.200.01.11>
- Storey, C.D., Jeffries, T.E. and Smith, M. 2006. Common lead-corrected laser ablation ICP-MS U–Pb systematics and geochronology of titanite. *Chemical Geology*, **227**, 37–52, <https://doi.org/10.1016/j.chemgeo.2005.09.003>
- Strachan, R.A., Alsop, G.I., Ramezani, J., Fraser, R.E., Burns, I.M. and Holdsworth, R.E. 2020a. Patterns of Silurian deformation and magmatism related to ductile thrusting in the northern Scottish Caledonides. *Journal of the Geological Society, London*, **177**, 893–910, <https://doi.org/10.1144/jgs2020-039>
- Strachan, R.A., Johnson, T.E., Kirkland, C.L., Kinny, P.D. and Kusky, T. 2020b. A Baltic heritage in Scotland: basement terrane transfer during the Grenville Orogeny. *Geology*, **48**, 1094–1098, <https://doi.org/10.1130/G47615.1>
- Strachan, R.A., Prave, A.R., Krabbendam, M. and Smith, M. 2024. Late Mesoproterozoic to Middle Neoproterozoic sedimentation and orogeny. In: Smith, M. and Strachan, R.A. (eds) *The Geology of Scotland*, 5th edn. Geological Society, London, in press.
- Tegner, C., Andersen, T.B. *et al.* 2019. A Mantle Plume Origin for the Scandinavian Dyke Complex: a ‘Piercing Point’ for 615 Ma plate reconstruction of Baltica? *Geochemistry, Geophysics, Geosystems*, **20**, 1075–1094, <https://doi.org/10.1029/2018GC007941>
- Tera, F. and Wasserburg, G.J. 1972. U–Th–Pb systematics in lunar highland samples from the Lunar 20 and Apollo 16 missions. *Earth and Planetary Science Letters*, **17**, 36–51, [https://doi.org/10.1016/0012-821X\(72\)90257-9](https://doi.org/10.1016/0012-821X(72)90257-9)
- Thigpen, J.R., Ashley, K.T., Mako, C., Law, R.D. and Spencer, B. 2021. Interplay between crustal-scale thrusting, high metamorphic heating rates, and the development of inverted thermal-metamorphic gradients: numerical models and examples from the Caledonides of Northern Scotland. *Tectonics*, **40**, e2021TC006716, <https://doi.org/10.1029/2021TC006716>
- Thomson, S.N., Gehrels, G.E., Ruiz, J. and Buchwaldt, R. 2012. Routine low-damage apatite U–Pb dating using laser ablation-multicollector-ICP-MS. *Geochemistry, Geophysics, Geosystems*, **13**, 1–23, <https://doi.org/10.1029/2011GC003928>
- Ueda, K., Gerya, T.V. and Berg, J.-P. 2012. Delamination in collisional orogens: thermomechanical modelling. *Journal of Geophysical Research*, **117**, B08202, <https://doi.org/10.1029/2012JB009144>
- Vance, D., Strachan, R.A. and Jones, K.A. 1998. Extensional versus compressional settings for metamorphism: garnet chronometry and P–T–t histories in the Moine Supergroup, northwest Scotland. *Geology*, **26**, 927–930, [https://doi.org/10.1130/0091-7613\(1998\)026<0927:EVCSFM>2.3.CO;2](https://doi.org/10.1130/0091-7613(1998)026<0927:EVCSFM>2.3.CO;2)
- Volante, S., Dziggel, A., Walters, J.B., Evans, N.J., Herbst, M. and Roper, R.A. 2023. Constraints on the Palaeoproterozoic tectono-metamorphic evolution of the Lewisian Gneiss Complex, NW Scotland: implications for Nuna assembly. *Journal of Metamorphic Geology*, **42**, 109–142, <https://doi.org/10.1111/jmg.12748>
- Walker, S., Thirlwall, M.F., Strachan, R.A. and Bird, A.F. 2016. Evidence from Rb–Sr mineral ages for multiple orogenic events in Caledonides of the Shetland Islands, Scotland. *Journal of the Geological Society, London*, **173**, 489–503, <https://doi.org/10.1144/jgs2015-034>
- Walker, S.F., Bird, A.F., Thirlwall, M.F. and Strachan, R.A. 2021. Timing and regional significance of Ordovician–Silurian orogenic events in Shetland, North Atlantic Caledonides: evidence from Lu–Hf and Sm–Nd garnet geochronology. *Geological Society, London, Special Publications*, **503**, 305–331, <https://doi.org/10.1144/SP503-2020-32>
- Wheeler, J., Park, R.G., Rollinson, H.R. and Beach, A. 2010. The Lewisian Complex: insights into deep crustal evolution. *Geological Society, London, Special Publications*, **335**, 51–79, <https://doi.org/10.1144/SP335.4>

- Whitehouse, M.J. 1989. Sm–Nd evidence for diachronous crustal accretion in the Lewisian Complex of Northwest Scotland. *Tectonophysics*, **161**, 245–256, [https://doi.org/10.1016/0040-1951\(89\)90157-1](https://doi.org/10.1016/0040-1951(89)90157-1)
- Whitehouse, M.J. 1993. Age of the Corodale gneisses, South Uist. *Scottish Journal of Geology*, **29**, 1–7, <https://doi.org/10.1144/sjg29010001>
- Whitehouse, M.J. and Bridgewater, D. 2001. Geochronological constraints on Palaeoproterozoic crustal evolution and regional correlations of the northern Outer Hebridean Lewisian complex, Scotland. *Precambrian Research*, **105**, 227–245, [https://doi.org/10.1016/S0301-9268\(00\)00113-3](https://doi.org/10.1016/S0301-9268(00)00113-3)
- Whitehouse, M.J. and Kemp, A.I.S. 2010. On the difficulty of assigning crustal residence, magmatic protolith and metamorphic ages to Lewisian granulites: constraints from combined *in situ* U–Pb and Lu–Hf isotopes. *Geological Society, London, Special Publications*, **335**, 81–101, <https://doi.org/10.1144/SP335.5>
- Whitehouse, M.J., Bridgewater, D. and Park, R.G. 1997. Detrital zircon ages from the Loch Maree Group, Lewisian Complex, NW Scotland: confirmation of a Palaeoproterozoic Laurentia–Fennoscandia connection. *Terra Nova*, **9**, 260–263, <https://doi.org/10.1111/j.1365-3121.1997.tb00025.x>
- Williams, I.S. 1998. U–Th–Pb geochronology by ion microprobe. *Reviews in Economic Geology*, **7**, 1–35.
- Xiang, D., Zhang, Z., Zack, T., Chew, D., Yang, Y., Wu, L. and Hogmalm, J. 2021. Apatite U–Pb dating with common Pb correction using LA-ICPMS/MS. *Geostandards and Geoanalytical Research*, **45**, 621–645, <https://doi.org/10.1111/ggr.12404>